

Key Points:

- We present and evaluate a novel model of dissolved Pb in the western Arctic Ocean
- The Canadian Arctic receives dissolved Pb from subpolar oceans and is a net sink
- Dissolved Pb traces warm Atlantic Water in Baffin Bay and to the West Greenland shelf

Supporting Information:

Supporting Information may be found in the online version of this article.

Correspondence to:

B. Rogalla,
brogalla@eoas.ubc.ca

Citation:

Rogalla, B., Allen, S. E., Colombo, M., Myers, P. G., & Orians, K. J. (2025). Modeling dissolved Pb concentrations in the western Arctic Ocean: The continued legacy of anthropogenic pollution. *Journal of Geophysical Research: Oceans*, 130, e2025JC022415. <https://doi.org/10.1029/2025JC022415>

Received 24 JAN 2025

Accepted 6 APR 2025

Author Contributions:

Conceptualization: B. Rogalla, S. E. Allen, M. Colombo
Funding acquisition: S. E. Allen, P. G. Myers, K. J. Orians
Investigation: B. Rogalla, S. E. Allen, M. Colombo
Methodology: B. Rogalla, S. E. Allen, M. Colombo, K. J. Orians
Software: B. Rogalla, P. G. Myers
Supervision: S. E. Allen, P. G. Myers, K. J. Orians
Visualization: B. Rogalla
Writing – original draft: B. Rogalla
Writing – review & editing: S. E. Allen, M. Colombo, P. G. Myers, K. J. Orians

© 2025. The Author(s).

This is an open access article under the terms of the [Creative Commons Attribution-NonCommercial-NoDerivs License](#), which permits use and distribution in any medium, provided the original work is properly cited, the use is non-commercial and no modifications or adaptations are made.

Modeling Dissolved Pb Concentrations in the Western Arctic Ocean: The Continued Legacy of Anthropogenic Pollution

B. Rogalla^{1,2} , S. E. Allen¹ , M. Colombo³, P. G. Myers⁴ , and K. J. Orians¹ 

¹University of British Columbia, Vancouver, BC, Canada, ²Now at British Antarctic Survey, Cambridge, UK, ³Virginia Institute of Marine Science, Gloucester Point, VA, USA, ⁴University of Alberta, Edmonton, AB, Canada

Abstract Over the past decade, the international GEOTRACES program has greatly expanded the coverage of dissolved lead (dPb) observations in the western Arctic Ocean including the Canada Basin and the Canadian Arctic Archipelago. However, it is difficult to quantify the drivers of the spatial distribution and seasonal variability of dPb concentrations using observations alone. Here, we present a three-dimensional model of dPb concentrations in the western Arctic Ocean with experiments from 2002 to 2021 to assess our current understanding of dPb cycling. The dPb model illustrates the impact of current and historical anthropogenic pollution on dPb concentrations in the Arctic Ocean, which accounts for at least 28% of dPb addition to the region, through aerosol deposition and net transport from other ocean basins. Advedted water masses from the Pacific and North Atlantic Oceans convey elevated pollution-derived dPb concentrations to the Arctic and play a key role, contributing 43% to the annual dPb budget. The Labrador Sea is a net source of dPb to Baffin Bay via the West Greenland Current. Within Baffin Bay, simulated dPb concentrations track the seasonal extension of warm Atlantic Water along the West Greenland shelf and occasional dense overflows of Atlantic Water into the deep Baffin Bay interior. While dPb concentrations in the western Arctic Ocean are low, the dPb model simulations presented here show that anthropogenic pollution continues to impact the Pb budget in this region, consistent with recent observational work, and demonstrate the use of dPb as a tracer of Atlantic and Pacific Water masses.

Plain Language Summary Over the past century, lead (Pb) concentrations in the atmosphere and ocean were dominated by pollution from leaded gasoline and industrial activity. While the Arctic Ocean is remote, it is connected to the Atlantic and Pacific Oceans, which receive more pollution. In the past decade, the number of observations of Pb in the western Arctic Ocean has greatly increased. Building on these observations, we created a new Pb model of the western Arctic Ocean and use it to assess our current understanding of Pb sources to the ocean. With experiments from 2002 to 2021, we showed that the Arctic Ocean, in particular its sediments, are a sink for Pb. We identified that present-day and historical pollution account for at least 28% of the Pb added annually to the western Arctic Ocean. Water from the Pacific and North Atlantic Oceans are a major supply of pollution-derived Pb to the region. Within Baffin Bay, Pb concentrations trace the seasonal inflow of warm Atlantic Water along the West Greenland shelf and into the deeper areas of Baffin Bay. While the western Arctic Ocean has low amounts of Pb, our model simulations suggest that pollution continues to impact the region, consistent with recent observations.

1. Introduction

Over the last century, the supply of lead (Pb) by anthropogenic pollution has strongly exceeded the natural supply (by crustal particles and volcanic gases) to the atmosphere, altering its cycling and resulting in serious human health consequences (Boyle et al., 2014; Nag & Cummins, 2022; Patterson & Settle, 1987a, 1987b; Schaule & Patterson, 1981). Pb emitted by ore smelting, as well as leaded gasoline and coal combustion, binds to aerosols that are dispersed and deposited to the ocean surface, conveying the signature from the atmosphere to the ocean (Bartoňová et al., 2019; Duce et al., 1991). As Pb is highly particle-reactive, dissolved Pb (dPb) is removed within <1–2 years in the upper ocean (Bacon et al., 1976; Kadko et al., 2019), but in the intermediate and deep ocean, the residence time of dPb increases to decades (Craig et al., 1973). As a result, the signature of anthropogenic Pb pollution can remain in the ocean for years and spread far away from the location of initial transfer to the ocean.

The historical anthropogenic pollution of Pb was centered on the North Atlantic and North Pacific Oceans (Boyle et al., 2014; Gobeil et al., 2001; Kelly et al., 2009; Schaule & Patterson, 1981). The North Atlantic Ocean saw the

highest dPb concentrations of all major ocean basins with peak concentrations of 200 pmol kg⁻¹ in ocean water in the 1970s; natural, preindustrial dPb concentrations in the Atlantic Ocean are estimated at 15 pmol kg⁻¹ (Kelly et al., 2009). Since then, the phaseout of leaded gasoline, scavenging removal, and mixing with more recently ventilated waters have decreased dPb concentrations in the global ocean (Pinedo-González et al., 2018). However, the historical signature of high dPb concentrations from the 20th century can still be found in intermediate and deep waters in the North Atlantic Ocean (Zurbrick et al., 2018). There is also evidence of continued input of dPb at the ocean surface from pollution in the North Pacific Ocean (Zurbrick et al., 2017). As a result of the exposure histories of water masses, Pb concentrations are a useful water mass tracer that incorporates information of when the water mass was ventilated (Colombo, Rogalla, et al., 2019; Gobeil et al., 2001).

The Arctic Ocean, while remote, has not been isolated from the impacts of Pb pollution as evidenced by the presence of anthropogenic Pb in aerosols (in particular during the winter Arctic haze period; Gong & Barrie, 2005; Sharma et al., 2019; Sturges & Barrie, 1989), snow and ice cores (Bory et al., 2014; Boutron et al., 1995; Pfirman et al., 1995; Rosman et al., 1993; Shotyk et al., 2005), and in the ocean (Colombo, Rogalla, et al., 2019; De Vera, Chandan, Pinedo-González, et al., 2021). At present, dPb concentrations in the Arctic Ocean are considered low (average of 5 pmol kg⁻¹); nevertheless, Pb isotope signatures suggest that anthropogenic pollution impacts the Arctic Ocean and surrounding land masses (Bory et al., 2014; Colombo, Rogalla, et al., 2019; De Vera, Chandan, Pinedo-González, et al., 2021). The Arctic Ocean receives waters enriched in dPb advected from the subpolar North Atlantic and North Pacific Oceans (Gobeil et al., 2001; Zurbrick et al., 2017), while the waters exiting the Arctic Ocean toward the North Atlantic Ocean through the Canadian Arctic Archipelago (CAA) are relatively depleted (Colombo, Rogalla, et al., 2019).

Over the past decade, observational campaigns associated with the GEOTRACES program have greatly expanded our knowledge of the cycling of Pb and Pb isotopes in the central Arctic Ocean (Bam et al., 2020; Charette et al., 2020; Kadko et al., 2019), the Chukchi Sea (M. Chen et al., 2012; Lepore et al., 2009; Vieira et al., 2019), the Canadian Arctic Ocean (Colombo, Rogalla, et al., 2019; De Vera, Chandan, Pinedo-González, et al., 2021), the North Atlantic Ocean (Krisch et al., 2022; Noble et al., 2015; Schlosser & Garbe-Schönberg, 2019; Zurbrick et al., 2018), and the North Pacific Ocean (Zurbrick et al., 2017). In fact, there were very few measurements of Pb concentrations in the Arctic Ocean prior to the GEOTRACES cruises (Boyle et al., 2014). Recent studies have also measured Pb concentrations in Arctic snow (Bolt et al., 2020), sea ice (Baskaran, 2005; Bolt et al., 2020), rivers (Colombo, Brown, et al., 2019), and the Greenland ice sheet (Hawkins et al., 2020; Krisch et al., 2022). With these new observations, we can attempt to constrain dPb cycling and spatial distributions in the Arctic Ocean using a model.

To the best of our knowledge, no three-dimensional ocean model of dPb exists that incorporates anthropogenic sources for the Arctic Ocean or globally. A few studies have used models to improve our understanding of Pb cycling in the oceans. Spencer et al. (1981) developed two-dimensional models of ²¹⁰Pb, an isotope of Pb not significantly perturbed by pollution, in the Atlantic Ocean to investigate boundary scavenging. Henderson and Maier-Reimer (2002) developed a global ocean model of ²¹⁰Pb and identified a near-surface maximum in natural dPb concentrations and order of magnitude variations in Pb residence times. More recently, M. Chen, Carrasco, et al. (2023) used a one-dimensional model of Pb and observations of dPb and Pb isotopes to suggest that particle-dissolved fluvial exchange is an important source of dPb to the oceans globally. Building on work by Wu et al. (2010), Lanning et al. (2023) illustrated reversible exchange of anthropogenic Pb isotopes using a simple box model. These models have improved specific aspects of our understanding of Pb cycling in the ocean; however, they are not able to provide a spatial view of the extent of anthropogenic pollution and contributions of a diverse set of sources.

In this paper, we present a time-varying, deterministic, three-dimensional model of dissolved Pb (dPb) in the western Arctic Ocean, extending from the Canada Basin through the shallow CAA to Baffin Bay. This model is embedded within a fully time-varying three-dimensional dynamical model. The dPb model incorporates novel parameterizations of sources and sinks of dPb that include seasonal variability, and a novel approach to estimating the dPb model boundary conditions based on the water masses present. With these parameterizations, the dPb model calculates how concentrations evolve over time and can thereby elucidate how dPb cycling may vary seasonally. With model simulations, we explore and extend the current understanding of dPb cycling in the western Arctic Ocean, illustrating the importance of net dPb transport from other ocean basins to the Canadian Arctic, the significant role of particulates in runoff and resuspension on the dPb budget, and the continued

contributions of atmospheric pollution. Lastly, using dPb as tracer, we highlight Atlantic Water pathways in Baffin Bay, a potential source of heat to marine-terminating glaciers on the west Greenland shelf.

2. Methods

We present a model of dissolved Pb (dPb) that runs offline with ocean and sea ice dynamics from the 1/12° Arctic and Northern Hemispheric Atlantic configuration (ANHA12; X. Hu et al., 2018) of the Nucleus for European Modeling of the Ocean version 3.6 (NEMO; Madec, 2008) with the Louvain-la-Neuve sea ice model (LIM2; Bouillon et al., 2009; Fichefet & Maqueda, 1997). The ANHA12 configuration has 50 vertical levels, and the 1/12° horizontal resolution corresponds to about 3–4 km in the CAA. Terrestrial runoff is based on monthly climatology and around Greenland, surface runoff is enhanced to include the impact of glacial melt (Bamber et al., 2012; Dai et al., 2009), and is held constant after 2010 (with a seasonal cycle). The ocean surface is forced with hourly atmospheric data from the Canadian Meteorological Centre's global deterministic prediction system (G. C. Smith et al., 2014), and tides are not explicitly included. For further details on the ANHA12 configuration, see Courtois et al. (2017) and X. Hu et al. (2018, 2019).

The dPb model consists of parameterizations for the addition and removal of dPb, and the advection and diffusion of dPb is calculated by the NEMO-TOP engine (Gent et al., 1995; Lévy et al., 2001). The model experiments run from January 2002 to December 2021 using 5-day-averaged dynamics fields. The dPb model is calculated on a subdomain of ANHA12, while the physical dynamics are from the full domain (Figure 1). In the following subsections, we describe the dPb model initial and boundary conditions, parameterizations, tuning, and experiments.

2.1. Initial and Boundary Conditions

The dPb model initial and boundary conditions are carefully designed to account for the historical signature of Pb pollution in water masses (see Text S1 in Supporting Information S1 for further details; Figure 2; Figures S1 and S2 in Supporting Information S1). We identify water masses based on their temperature and salinity, and associate the water masses with dPb concentrations from observations (Figure 2; Colombo, Rogalla, et al., 2019; Zurbrick et al., 2018). The dPb concentrations associated with each water mass are kept constant over time due to the lack of available seasonal dPb observations; however, our method accounts for the seasonal variation in inflow of water masses. Then, we construct a mapping from temperature and salinity to dPb concentrations (Figure S1 in Supporting Information S1; details in Text S1 in Supporting Information S1). For the initial conditions, this mapping is applied to ANHA12 salinity and temperature fields from January 2002 (Figure S2 in Supporting Information S1). For each boundary, the ANHA12 temperature and salinity are used in the mapping to set the dPb concentration at the boundary for each month (Figure 2; Figure S3 in Supporting Information S1). The water masses considered in the initial and boundary conditions, and their observed dPb concentrations, are described next.

The Labrador Sea boundary receives low dPb concentration (5–10 pM) Arctic outflow from the southward Baffin Island Current (Colombo, Rogalla, et al., 2019). Along the Greenland slope, warmer and saltier Atlantic (Irminger) Water flows northward via the West Greenland Current (WGC), carrying high dPb concentrations (25–30 pM; Colombo, Rogalla, et al., 2019; Zurbrick et al., 2018). The recirculation of the WGC in Davis Strait delivers intermediate dPb concentrations (15–20 pM) to the central Labrador Sea boundary (Colombo, Rogalla, et al., 2019). Deep waters have low dPb concentrations (5 pM) as they have not been exposed to historical pollution and have undergone removal through scavenging (Colombo, Rogalla, et al., 2019; Noble et al., 2015).

At the Arctic Ocean boundaries, dPb concentrations in the polar mixed layer (PML) are low (<5 pM; Colombo, Rogalla, et al., 2019), while the Pacific-derived Alaskan Coastal Water (ACW) supplied by the Alaskan Coastal Current (ACC) has elevated dPb concentrations (9–16 pM; Colombo, Rogalla, et al., 2019). Cold and fresh winter Bering Sea water is associated with very low dPb concentrations (3–5 pM; Colombo, Rogalla, et al., 2019). The warmer and saltier Atlantic layer has elevated dPb concentrations (5–7 pM; Colombo, Rogalla, et al., 2019). As in Baffin Bay, Canada Basin deep waters have low dPb concentrations (3 pM; Colombo, Rogalla, et al., 2019).

dPb concentrations at the Hudson Bay boundary cannot be constrained with observations. Instead, we assume that Arctic outflow dominates dPb concentrations in this region and that Hudson Bay does not have significant local sources of pollution, and apply dPb concentrations from the Arctic Ocean water mass end-members. dPb

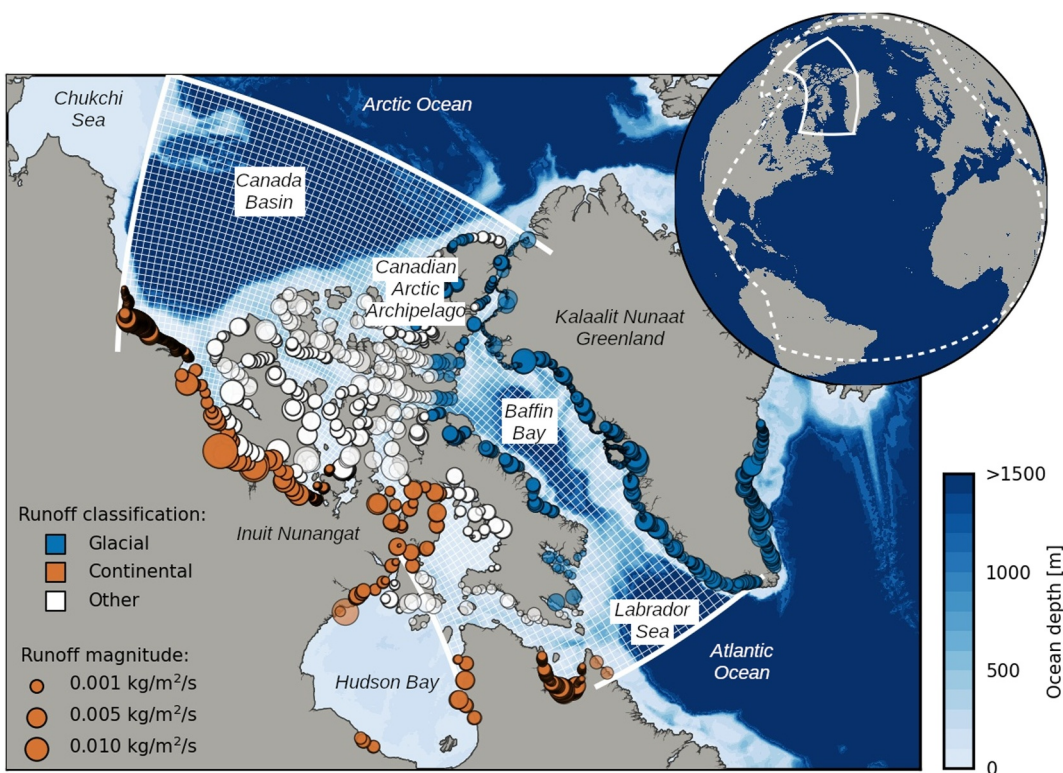


Figure 1. The dPb model domain, delineated with a solid white line, extends from the Canada Basin to the Labrador Sea with 2–3 km resolution in the southern Canadian Arctic Archipelago and 3–4 km in Baffin Bay. Thin white lines mark one in every 10 grid points. The dashed line in the inset globe delineates the full domain of the Arctic and Northern Hemispheric Atlantic configuration (ANHA12; X. Hu et al., 2018). Terrestrial runoff sources are marked with size proportional to September 2010 discharge forcing and colored based on the assigned drainage basin category: glacial (blue), continental (orange), or other (white).

concentrations in sediment core samples in Hudson Bay suggest relatively constant dPb concentrations over the last century, but isotopic signatures do indicate an increase in the relative proportion of anthropogenic lead in Hudson Bay (Thibodeau et al., 2017). The modeled dPb concentrations in Baffin Bay are not sensitive to the choice of the Hudson Bay boundary condition concentrations as water flows through Hudson Strait and southward along the coast of Labrador out of the dPb model domain (Figure S4 in Supporting Information S1).

2.2. Parameterizations of Dissolved Pb Sources and Sinks

Dissolved Pb is removed from the water column through scavenging onto particulates and can be added by deposition of natural and anthropogenic aerosols, terrestrial runoff, sediment resuspension, and release from sea ice (Baskaran, 2005; Colombo, Brown, et al., 2019; Colombo, Rogalla, et al., 2019; Noble et al., 2015; Patterson & Settle, 1987b; Schlosser & Garbe-Schönberg, 2019). Below, we describe the parameterizations of these processes (parameters in Table 1); the parameterizations for aerosol flux, sediment resuspension, and sea ice follow a similar approach as for the Arctic Mn model in Rogalla et al. (2022). The supply of dPb by hydrothermal fluids is excluded as a source within the study domain as there are no significant local sources of hydrothermal fluids and dPb is typically removed rapidly nearby vents (J. H. Chen et al., 1986; German et al., 1991; Noble et al., 2015).

2.2.1. Scavenging Removal

Dissolved Pb is highly particle-reactive and adsorbs to lithogenic, authigenic, and biogenic particle surfaces (Chuang et al., 2014; Grousset et al., 1995; Lambert et al., 1991; Luengen et al., 2007; Schlosser & Garbe-Schönberg, 2019). This Pb is subsequently removed to the sediments by particle settling. Pb scavenging is most efficient in productive coastal and continental shelf regions where particles are abundant (M. Chen et al., 2012; Luengen et al., 2007; Schlosser & Garbe-Schönberg, 2019). Scavenging shapes the residence time of dPb in the

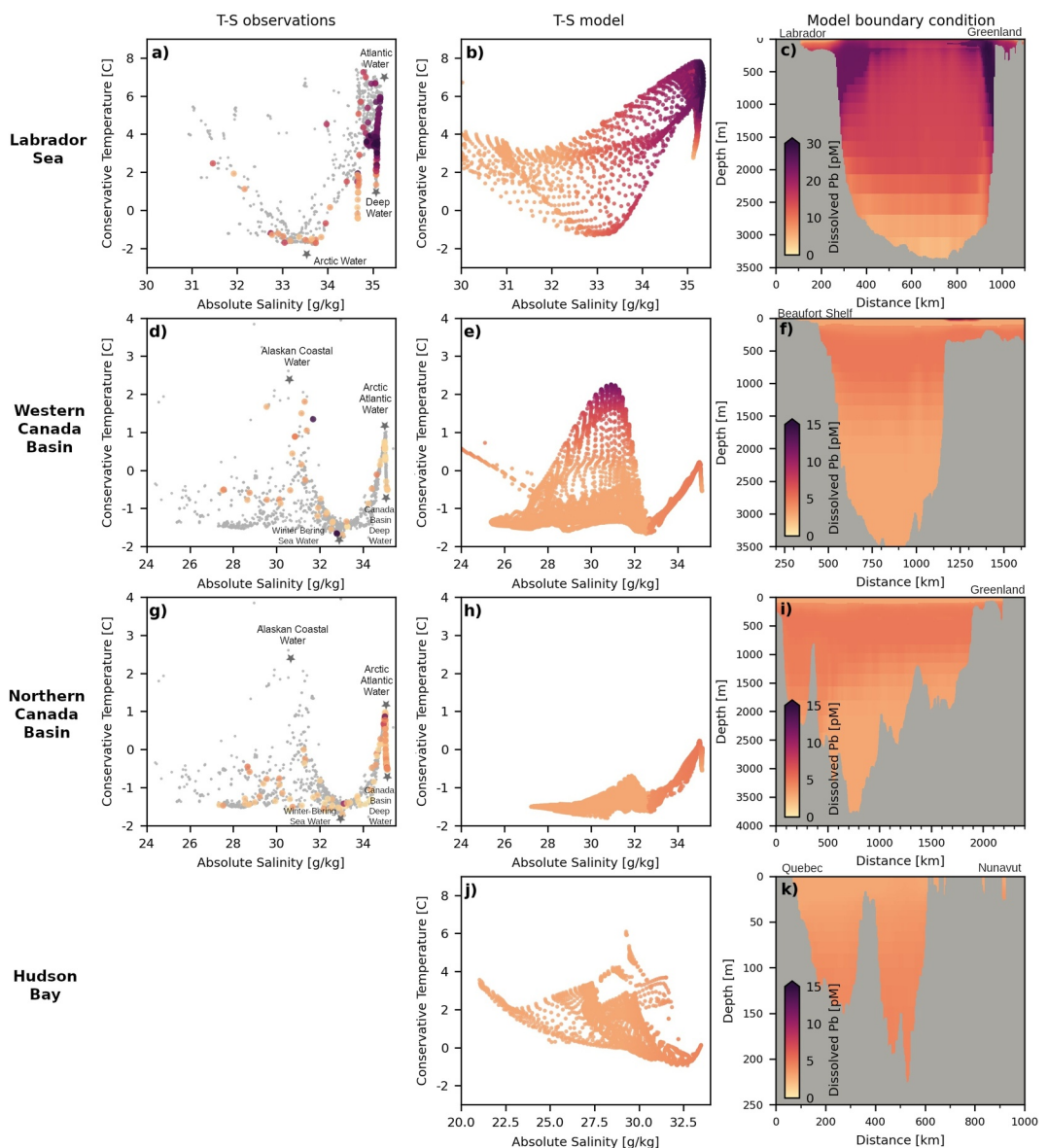


Figure 2. The dissolved Pb (dPb) model boundary conditions (locations marked in Figure 1) are created by identifying water masses from modeled temperature and salinity and pairing them with dPb concentrations observed in these water masses (in this figure; Figure S1 and Text S1 in Supporting Information S1). Each row in this figure specifies a boundary location. The left column (panels a, d, g) shows temperature-salinity diagrams with dPb concentrations from GEOTRACES observations (GEOTRACES Intermediate Data Product Group, 2021), with the color bars included in the rightmost column. The middle column (panels b, e, h, j) shows the dPb model boundary conditions in August 2015. The right column (panels c, f, i, k) shows transects of dPb concentrations in the model boundary conditions. Gray circular markers in panels (a), (d), and (g), indicate measured temperature and salinity at locations without dPb samples, and water mass end-members are marked with their name and a star. Note that the color bar scale for the Labrador Sea extends to higher concentrations, and that the temperature, salinity, and depth ranges differ between panels.

ocean; residence times vary from several months to 2 years in the surface, up to decades in intermediate and deep waters (Bacon et al., 1976; Henderson & Maier-Reimer, 2002; Nozaki et al., 1976).

In this model, dPb is removed by irreversible scavenging onto particle fields at a rate described by:

$$\left. \frac{\partial [dPb]}{\partial t} \right|_{scavenging} = -(\beta \cdot P_{litho,authigenic} + (1 - \beta) \cdot P_{biogenic}) \cdot k_p \cdot [dPb] \quad (1)$$

Table 1*Constants and Parameter Values Used in Dissolved Lead (Pb) Model Experiments*

Parameter	Description	Value	Source
α_0	Fractional solubility of Pb at 4°C	0.80	Fishwick et al. (2018)
m	Molar mass of Pb	207.2 g mol ⁻¹	—
$f_{Pb\ crust}$	Natural Pb fraction in Earth's crust	17 ppm	Gobeil et al. (2001) and Wedepohl (1995)
$f_{Pb:BC}$	Aerosol Pb to black carbon ratio	0.011	This study ^a
k_p	Scavenging rate constant	$5 \cdot 10^{-6} \text{ s}^{-1}$	This study
β	Fraction lithogenic and authigenic particles	0.10	This study
C	Tidal erosion tuning constant	$1.2 \cdot 10^{-8}$	This study
γ	Solubility parameter	0.065	Rogalla et al. (2022)
ϵ	Estuarine particle transfer efficiency	0.15	This study
D_{class}, S_{class}	Runoff (dissolved Pb and particulate matter)		This study ^b
	- Glacial	35 pM and 261 mg L ⁻¹	
	- Continental	43 pM and 12 mg L ⁻¹	
	- Other	2 pM and 4 mg L ⁻¹	

^aWith observations from Alert, Nunavut from Sirois and Barrie (1999) and Gong et al. (2010). ^bWith observations from Colombo, Brown, et al. (2019) and Brown et al. (2020).

where $[dPb]$ is the concentration of dissolved Pb, β is the fraction of lithogenic and authigenic particles, $P_{litho,authigenic}$ is the spatial field of combined lithogenic and authigenic particle abundance (normalized by the maximum abundance observed within the domain over the full time series), $P_{biogenic}$ is a modified normalized biogenic particle abundance (calculated per Equation 2), and k_p is the scavenging rate constant. The parameters β and k_p are tuned by optimizing the combination that best represents observed dPb residence times (Section 2.3). We set the scavenging rate constant to be the same for all particle types as differential scavenging efficiency depending on particle chemistry is currently difficult to constrain based on available observations. Note that the tuned parameter β does however indirectly incorporate preferential adsorption to different particle types because it scales the magnitude of the biogenic versus lithogenic and authigenic particle fields. There are also indications that Pb is reversibly scavenged from particles in deep basins (Boyle et al., 2020; Wu et al., 2010). However, similar to Henderson and Maier-Reimer (2002), we do not incorporate the effect of reversible scavenging into this dPb model as this is expected to be small, consistent with observed deep Pacific Ocean dPb concentrations (Lanning et al., 2023).

Biogenic particle fields, P_{bio} , are calculated monthly from the sum of phytoplankton biomass and particulate organic phosphate content derived from the vertical particulate organic phosphate flux and the sinking rate of a 1/4° NEMO configuration with the BLING model (Castro de la Guardia, 2018; Galbraith et al., 2010). The sinking material is a combination of sinking algal cells and aggregates, and zooplankton fecal matter. The modified normalized biogenic particle abundance, $P_{biogenic}$, takes into account the relationship between scavenging onto biogenic particles and particle size as follows:

$$P_{biogenic} = \frac{P_{bio}}{\max(P_{bio})^{0.85}} \quad (2)$$

where the exponent, 0.85, is derived from the power-law relationship between suspended particulate matter and the Pb partitioning coefficient in Bam et al. (2020) and limits the scavenging by the largest particles. The maximum of the biogenic particle fields, $\max(P_{bio})$, is the maximum abundance anywhere over the full time series. We estimate the monthly combined lithogenic and authigenic particle field based on oxidized Mn from an Arctic Mn model (Rogalla et al., 2022), as oxidized Mn is an effective scavenger and Pb is likely scavenged by Mn oxides (Bam et al., 2020; Hollister et al., 2020). The biogenic particle field dominates behavior in the upper 50–200 m, while the lithogenic particle field is more important below that, consistent with Xiang and Lam (2020).

2.2.2. Direct Aerosol Deposition and Indirect Release From Sea Ice

Aerosols contribute Pb to the ocean through direct (dry and wet) deposition, Φ_{atm} , and through release during sea ice melt, Φ_{ice} . In the Arctic, aerosol Pb comes from natural crustal sources and from anthropogenic pollution (De Vera, Chandan, Landing, et al., 2021; Sharma et al., 2019).

In the dPb model, the natural aerosol contribution is estimated from dust deposition and the fraction of Pb in the continental crust. The pollution origin aerosol contribution is estimated using black carbon, as black carbon flux model products are more readily available, and both black carbon and lead are produced during the combustion of fossil fuels (Macdonald et al., 2000). The fraction of Pb aerosols relative to black carbon aerosols, $f_{Pb\ BC}$, is estimated from observations in Alert, Nunavut from 1989 to 1992 (see Text S2 and Figure S5 in Supporting Information S1; Gong et al., 2010; Sirois & Barrie, 1999). More recent observations in Alert indicate that while aerosol Pb and black carbon concentrations have decreased by 56% and 52%, respectively, since the 1990s, their ratio is not significantly altered (Sharma et al., 2019). The contribution to dPb from natural and pollution-origin aerosols can be written as follows:

$$\frac{\partial[dPb]}{\partial t} \Big|_{atm\ or\ ice} = \frac{\alpha_0 \cdot f_{Pb\ aerosol}}{m \cdot \Delta z_{surface}} \cdot \Phi_{aerosol\ atm\ or\ ice} \quad (3)$$

where α_0 is the fractional solubility of Pb, m is the molar mass of Pb, and $\Delta z_{surface}$ is the surface grid cell thickness. The fraction of Pb contributed by the aerosol, $f_{Pb\ aerosol}$, is either the mass fraction of Pb in the continental crust ($f_{Pb\ crust}$) or the fraction of pollution-origin Pb in aerosols (f_{PbBC}), for the natural and pollution-origin aerosol contributions, respectively. Similarly, $\Phi_{aerosol}$ refers to either the dust or black carbon fluxes for the natural and pollution-origin aerosol contributions. The monthly atmospheric and sea ice dust and black carbon fluxes are interpolated onto the ANHA12 grid from postprocessed atmospheric data from an ensemble member (LE2-1001) of the Community Earth System Model (CESM2) Large Ensemble experiments (Danabasoglu et al., 2022; Rodgers et al., 2021).

2.2.3. Terrestrial Runoff

River discharge and glacial melt contribute Pb to the shelf seas (M. Chen, Carrasco, et al., 2023; Colombo, Rogalla, et al., 2019; Krause et al., 2023; Krisch et al., 2022; Schlosser & Garbe-Schönberg, 2019). However, the exact contribution is challenging to constrain as the cycling of Pb (due to scavenging, flocculation, and particle settling) at the river-ocean interface is complex and varies between estuaries (Henderson & Maier-Reimer, 2002; Elbaz-Poulichet et al., 1984; Schlosser & Garbe-Schönberg, 2019, and references therein). dPb released during weathering of glacial flour can be quickly removed by sorption on particle surfaces, so the proportion removed is sensitive to the suspended sediment load (Krause et al., 2023; Schlosser & Garbe-Schönberg, 2019). Mixing also remobilizes particles including particulate Pb, and this increased turbidity results in enhanced adsorption of dPb to particles and enhanced removal through flocculation and scavenging (Duinker, 1983; Elbaz-Poulichet et al., 1984; Jiann et al., 2005).

The physical model and the dPb model used in this study can not resolve the spatial scale of the processes at the river-ocean interface. Instead, dPb supply by runoff is estimated based on the dissolved Pb fraction and the indirect contribution from suspended particulate matter with a transfer efficiency of ϵ . The dPb contribution from runoff depends on the discharge rate, Q , and on properties of the catchment basin (Colombo, Brown, et al., 2019). Each runoff source is assigned a class (Figure 1) with an associated characteristic dPb concentration, D_{class} , and suspended particulate matter content, S_{class} , based on observations (Table 1; Brown et al., 2020; Colombo, Brown, et al., 2019; Rogalla et al., 2023). The runoff contribution is calculated as follows:

$$\frac{\partial[dPb]}{\partial t} \Big|_{runoff} = \frac{Q}{\rho_0 \cdot \Delta z_{surface}} \left(D_{class} + \epsilon \frac{S_{class} \cdot \alpha_0 \cdot f_{Pb\ crust}}{m} \right) \quad (4)$$

where ρ_0 is the density of freshwater. Glacial melt enters the ocean through direct discharge and through sub-glacial melt plumes (Bhatia et al., 2021); the model is unable to resolve entrainment at the glacier mouth, but

includes glacial melt in runoff. The glacial (35 pM) and continental (43 pM) dissolved Pb runoff concentrations from Colombo, Brown, et al. (2019) are lower than, but comparable to, the dPb end-member of 54 ± 7 pM in glacial runoff observed in a Greenland fjord (Krisch et al., 2022).

2.2.4. Sediment Resuspension

Dissolved Pb can increase near the ocean floor as a result of sediment resuspension (M. Chen et al., 2012; De Vera, Chandan, Pinedo-González, et al., 2021; Noble et al., 2015). However, sediment resuspension can also enhance adsorptive removal of particle-reactive dPb and thereby reduce concentrations near the seafloor (Colombo, Rogalla, et al., 2019; Kuzyk et al., 2013; Lepore et al., 2009; Spencer et al., 1981). Generally, the biogeochemical processes controlling sedimentary release of dPb are poorly constrained (Vieira et al., 2019).

In this dPb model, sediment resuspension is incorporated as a continuous process based on tidal stress (Figure S6 in Supporting Information S1) calculated from the barotropic tidal speed, U_{tidal} , as follows:

$$\frac{\partial[d\text{Pb}]}{\partial t}\Big|_{\text{sediment}} = C \cdot U_{tidal}^2 \cdot \frac{\alpha_0 \gamma (1 - e^{-U_{tidal}^2/\gamma})}{U_{tidal}^2} \cdot \frac{f_{\text{Pb crust}}}{m \cdot \Delta z_{bottom}} \quad (5)$$

where the tidal erosion tuning constant, C , sets the overall strength of the contribution of resuspension for dPb, and the solubility parameter, γ , modifies the solubility so that the resuspension rate has an upper limit at high tidal speeds (Rogalla et al., 2022). We use the barotropic tidal speeds from the MOG2D-G model (Carrère & Lyard, 2003). The fraction of Pb in the continental crust, $f_{\text{Pb crust}}$, is the same as used in the other equations. However, the fraction of Pb in seafloor sediments could be higher than the typical continental crust fraction, as deposited sediments on the seafloor are enriched with anthropogenic Pb (De Vera, Chandan, Pinedo-González, et al., 2021). On the other hand, the crustal fraction used is on the upper end of the range observed in the Chukchi Sea by Cai et al. (2011).

2.2.5. Sediment Entrained in Sea Ice and Subsequent Melt

Sea ice-rafted sediments have been identified as a source of ^{210}Pb , a nonanthropogenic Pb isotope, and other trace elements to the ocean surface (Baskaran, 2005; M. Chen et al., 2012; Rogalla et al., 2022) and dPb concentrations as high as 33 pM have been measured in Arctic sea ice melt ponds (Marsay et al., 2018).

In the dPb model, we estimate the contribution from sea ice by coupling the Pb contained in sediments in sea ice and the sea ice melt rate, I_{melt} , similar to Rogalla et al. (2022) as follows:

$$\frac{\partial[d\text{Pb}]}{\partial t} = \frac{\alpha_0 \cdot f_{\text{Pb crust}}}{m \cdot \Delta z_{surface}} \cdot S_e \cdot I_{melt} \quad (6)$$

where S_e is the effective sediment content at each grid point. The effective sediment content is spatially variable, and depends on the amount of sediment that was incorporated during ice formation on the shelves and on sea ice transport. The effective sediment content is multiplied by a tuning constant to account for the net effect of enhanced particle-reactive Pb removal (see Section 2.3). The above parameterization assumes that Pb released by sea ice originates from shelf sediments in the particulate form and that during melt, these particles undergo dissolution. We also focus the parameterization on the particulate component because much of the sea ice in our domain is multi-year ice, and we assume that most of the dPb in sea ice drains from the ice matrix early in the melt season alongside the sea ice brine. The spatial variation in the sediment content in sea ice is estimated based on the proportion of sea ice in the Canada Basin that formed over the Siberian shelves during stormy fall months, estimated using particle tracking (Figure S7 in Supporting Information S1; see Rogalla et al., 2022, for details).

2.3. Tuning

The tuned parameters in the dPb model are the scavenging rate (k_p), fraction of lithogenic and authigenic particles (β), estuarine particle transfer efficiency (ϵ), tidal erosion constant (C), and effective sediment content in sea ice (S_e). The scavenging removal of dPb is tuned by estimating the parameter combination of k_p and β that most

Table 2*Description of Model Forcing for the Dissolved Lead (dPb) Model Experiments*

Experiment name	Description of forcing change	Period
Reference	—	2002–2021 ^a
Labrador Atlantic	Increase [dPb] in Atlantic Water at the Labrador Sea boundary	2002–2021 ^a
Hudson Bay	Increase [dPb] at the Hudson Bay boundary	2002–2007 ^a

^aPrior to the study period, the model is spun up by repeating the year 2002 nine times.

closely captures the observed patterns in dPb residence time in the Arctic Ocean and sub-Arctic North Atlantic and North Pacific Oceans (Baskaran et al., 2022; M. Chen et al., 2012; Chung & Craig, 1983; Cochran et al., 1990, 1995; W. Hu et al., 2014; Kadko et al., 2019; Moore & Smith, 1986; Nozaki et al., 1976, 1997; J. N. Smith et al., 2003). The residence time of dPb in the model is estimated over the course of a year from the ratio of the monthly dPb inventory to the monthly removal, assuming steady-state conditions. With the scavenging removal set, we ran a tuning experiment with spin-up from 2002 to 2010 and branched four experiments from 2010 to 2015: one with all components on and best-guess parameter values and the others with $\epsilon = 0$, $C = 0$, and $S_e = 0$ respectively. For each of these experiments, we compared simulated dPb concentrations relative to the best guess with observed dPb concentrations from Colombo, Rogalla, et al. (2019). Assuming that the dPb concentrations in specific regions are nearly linear in these parameters, we can tune the parameters based on these experiments. From the particulate matter in runoff experiment, we estimate ϵ based on simulated dPb concentrations in the upper water column in Lancaster Sound and in Baffin Bay. From the sediment resuspension experiment, we estimate C based on the near-bottom observed dPb concentrations in coastal regions in the CAA. From the sea ice melt off experiment, we estimate S_e based on the upper water column dPb concentrations in regions away from the coastline and strong advective signals (primarily in the Canada Basin).

2.4. Experiments

We perform a reference experiment and two sensitivity experiments with the dPb model (experiments summarized in Table 2). The sensitivity experiments establish the impact of the specification of dPb concentrations at the Labrador Sea and Hudson Bay boundaries on dPb concentrations in the study domain. In addition, the “Labrador Atlantic” experiment maps pathways of Atlantic Water in Baffin Bay. In the Labrador Atlantic experiment, dPb concentrations are increased from 30 to 35 pM for the Atlantic Water end-member. In the “Hudson Bay” experiment, dPb concentrations are increased from 3 to 5 pM for the PML end-member and from 5 to 10 pM in the Atlantic Water end-member. We run the Hudson Bay experiment from 2002 to 2007 as this period is long enough to establish that the Hudson Bay boundary does not impact the interior of the domain. The dPb model experiments are spun up by repeating the year 2002 nine times; at this point, the year-to-year profile changes at evaluation stations are small and Atlantic influence extends throughout Baffin Bay (Figure S8 in Supporting Information S1).

3. Results

3.1. Dissolved Pb Model Evaluation

We evaluate the dissolved Pb (dPb) model with observations collected by the GEOTRACES GN01, GN02, and GN03 cruises in the Arctic Ocean between 3 August and 28 September 2015 (Colombo, Rogalla, et al., 2019; GEOTRACES Intermediate Data Product Group, 2021). These dPb observations highlighted a few key features (Colombo, Rogalla, et al., 2019): a gradient in dPb concentrations from the Arctic Ocean to the Labrador Sea, elevated dPb concentrations at 300–800 m depth in Baffin Bay in Atlantic Water from the Labrador Sea, and a separation in dPb characteristics west and east of Barrow Sill in the CAA. Within the Canada Basin and the western CAA, observations identified a peak in dPb at 50–100 m depth in Pacific-derived Alaskan Coastal Water from the Alaskan Coastal Current and weakly elevated dPb in Atlantic Water from Fram Strait. We focus the following model evaluation on three layers: the mixed layer (0–34 m depth), the subsurface layer (40–110 m depth), and the Atlantic layer (454–763 m depth).

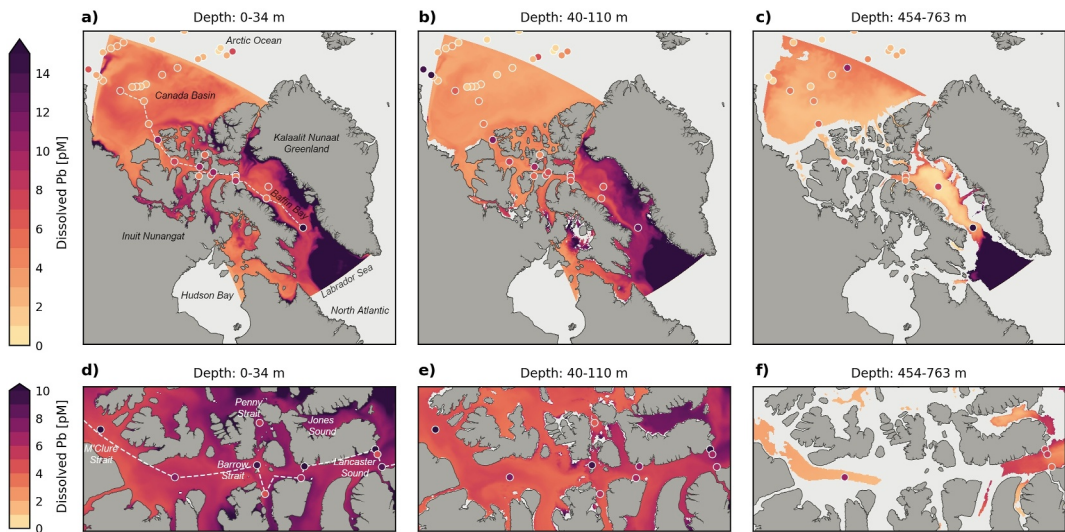


Figure 3. Dissolved Pb (dPb) concentrations in the mixed layer (a and d), subsurface layer (b and e), and Atlantic layer (c and f) in August–September 2015. The shading corresponds to modeled dPb concentrations averaged over the sampling time period (August–September 2015), and the circles indicate observed dPb concentrations from GEOTRACES GN01-03 cruises (GEOTRACES Intermediate Data Product Group, 2021). Observations are averaged over each layer's depth range, with a buffer of 15 m when shallower than 200 m and with a 50 m buffer otherwise. Panels (d–f) expand the Parry Channel region of the Canadian Arctic Archipelago. Note the difference in color bar scale for panels (a–c) and (d–f). Areas masked as land in the dPb model are indicated in light gray and are masked based on the shallowest depth in the layer's depth range. The white dashed line in panels (a and d) indicates the path of the transect shown in Figure 4.

The model captures the overall observed magnitude of, and increase in, dPb concentrations from the Canada Basin to the Labrador Sea (Figures 3 and 4). Modeled dPb concentrations in the mixed layer are lowest in the Canada Basin (3–7 pM), increase as waters transit through the CAA (4–9 pM) into central Baffin Bay (7–10 pM), and are highest in the Labrador Sea (14–26 pM). Modeled dPb concentrations in the mixed layer are elevated along coastlines near runoff sources, especially in the glaciated areas of Greenland, Ellesmere Island, and Baffin Island (40–80+ pM). The magnitude of modeled dPb concentrations is comparable to observations in Colombo, Rogalla, et al. (2019) at stations that are affected by runoff, such as CAA1 in northern Lancaster Sound (affected by a glacial plume), and BB3 and BB1 along the Baffin Island coast. Observed dPb concentrations around West Greenland are elevated, but cover a broad range from 3.2 to 252 pM (Krause et al., 2023); there are currently not enough observations to constrain the model estimates of dPb near the Greenland ice sheet. However, the salinity-dPb relationship derived from observations near Nioghalvfjerdsbrae, a floating ice tongue on the Northeast Greenland shelf, suggests a freshwater dPb end-member of 54 ± 7 pM (Krisch et al., 2022), which falls within the same range as our simulations.

Atlantic Water from the Labrador Sea creates a distinct peak in simulated and observed dPb concentrations in the intermediate water column in Baffin Bay (Figures 3c and 4; Colombo, Rogalla, et al., 2019). However, the elevated dPb signal is weaker and shallower in the model (7–14 pM; 200–400 m depth) than observed (10–25 pM; 300–800 m depth; Colombo, Rogalla, et al., 2019), possibly due to excess adsorptive removal in the deeper water column in Baffin Bay in the model. Davis Strait is ~640 m deep, and its topography controls the inflow of Atlantic Water from the Labrador Sea into Baffin Bay. Slight deviations in the extension of high dPb content water from the Labrador Sea in the model also impact the representation of high dPb concentrations sampled at station BB1 (up to 27 pM) in Davis Strait (Figures 3a–3c and 4). As seen in the observations in western Baffin Bay (Colombo, Rogalla, et al., 2019), elevated dPb concentrations from Atlantic Water and from Greenland runoff are transported around Baffin Bay by the cyclonic WGC and combine with Arctic outflow in northern Baffin Bay (Figures 3a and 3b). The isopycnal surfaces associated with the dPb peak deepen along the path of the WGC and are associated with warm Irminger Water (Figure 4; Colombo, Rogalla, et al., 2019). In western Baffin Bay, lower dPb concentration Arctic outflow from Lancaster Sound, Jones Sound, and Nares Strait merges with recirculating WGC water and decreases observed and modeled concentrations offshore of Baffin Island (lower dPb plume visible in Figure 3b; Colombo, Rogalla, et al., 2019).

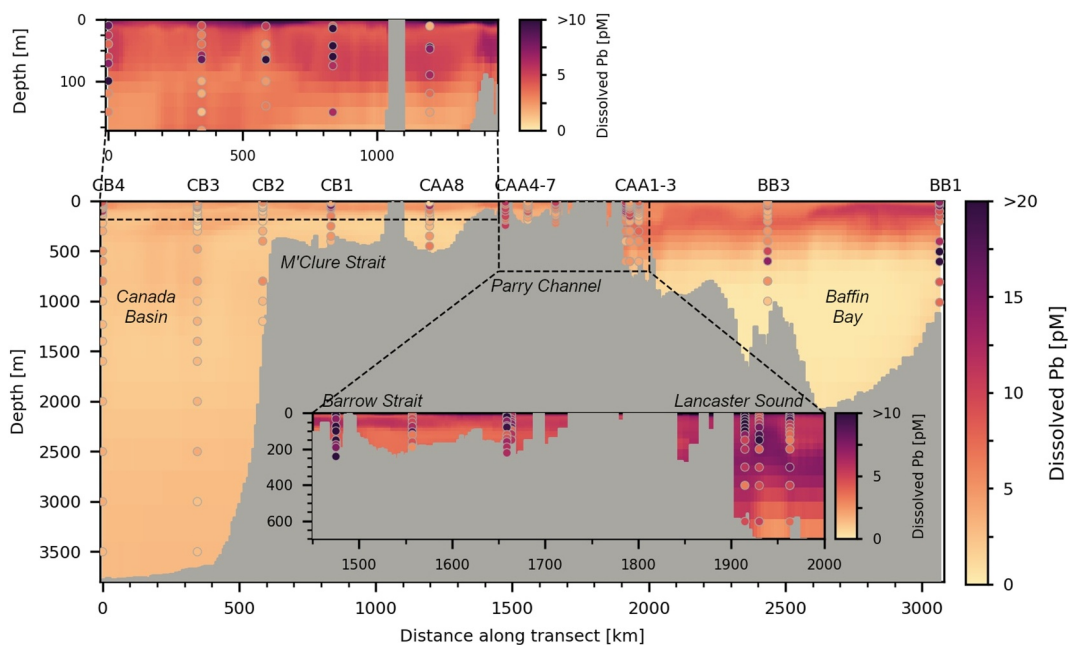


Figure 4. A transect of dissolved Pb (dPb) concentrations from the Canada Basin through Parry Channel in the Canadian Arctic Archipelago (CAA) to Baffin Bay (path is marked by a white dashed line in Figures 3a and 3d). The background shading corresponds to modeled dPb concentrations averaged over the sampling time period (August–September 2015), and the circles indicate observed dPb concentrations from GEOTRACES GN02-03 cruises (Colombo, Rogalla, et al., 2019). Station names are indicated above the main axes. The inset axes expand the upper water column in the Canada Basin and the western CAA (top inset), and the central and eastern Parry Channel region (center inset). Note that the color bar ranges are reduced for the inset axes.

Within the CAA, the model captures a change in dPb concentrations west and east of Barrow Strait (Figure 3e), consistent with observed patterns (Colombo, Rogalla, et al., 2019). The shallow sill (at ~120 m depth) in Barrow Strait limits the westward extension of recirculating high dPb Atlantic Water from Baffin Bay and the eastward flow of deeper waters from the Arctic Ocean in both the observations and the model (Figure 3; Colombo, Rogalla, et al., 2019). In Lancaster Sound, the model represents the elevated concentrations observed at CAA1 on the north side of the channel (up to 13 pM in the observations; Colombo, Rogalla, et al., 2019) and the lower concentrations observed in the Arctic outflow (4–5 pM; Colombo, Rogalla, et al., 2019), although the magnitude of the across-channel variation in the model is smaller than observed for the mixed layer (Figures 3d–3f; Colombo, Rogalla, et al., 2019). The model also captures the increase in dPb to 8 pM at 200–400 m depth in Lancaster Sound from recirculating Atlantic Water from Baffin Bay (Figure 4; Colombo, Rogalla, et al., 2019). In Barrow Strait (station CAA6), the model underestimates dPb concentrations at all depth levels (Figure 4; Colombo, Rogalla, et al., 2019). This region is characterized by strong mixing, and observed dPb concentrations at CAA6 are higher than any of the surrounding stations (7–11 pM compared to 3–8 pM), attributed to Atlantic Water from Baffin Bay (Colombo, Rogalla, et al., 2019; Hughes et al., 2017). The model may underestimate dPb here due to a difference in the westward extension of Atlantic Water from Lancaster Sound, or due to underestimation of a local source such as sediment resuspension.

In the Canada Basin and the western CAA (M'Clure Strait), the model captures the overall magnitude of dPb concentrations (Figure 4; Colombo, Rogalla, et al., 2019), but underestimates the observed dPb peak at 50–100 m depth associated with Pacific-derived Alaskan Coastal Water (ACW; Colombo, Rogalla, et al., 2019). Just outside the dPb model domain on the Chukchi shelf, higher dPb concentrations are observed. The western Canada Basin model boundary conditions appear to capture these concentrations; a plume of higher dPb water from the Chukchi shelf is simulated in the mixed layer and extends toward the Canada Basin, but the simulated subsurface peak is underestimated (Figure 3a). In the mixed layer in the Canada Basin, elevated dPb concentrations are simulated in regions with strong sea ice melt along the outer edges of the Beaufort Gyre (Figures 3a and 4), as noted in the observations at station CB4 (Colombo, Rogalla, et al., 2019).

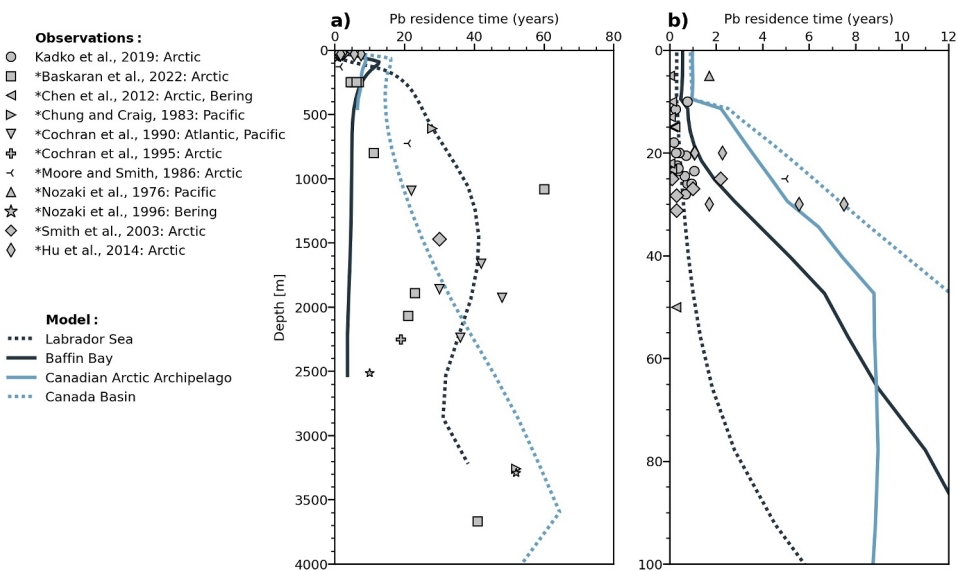


Figure 5. Average dissolved Pb (dPb) residence time in the model in the full water column (a) and zoomed in on the upper water column (b), calculated over the time series from 2002 to 2021 and separated by regions (solid and dotted lines; region definitions in Figure S9 in Supporting Information S1). Markers indicate Pb residence time estimates from observational studies in the Arctic Ocean and sub-Arctic seas with locations listed in the legend (Baskaran et al., 2022; M. Chen et al., 2012; Chung & Craig, 1983; Cochran et al., 1990, 1995; W. Hu et al., 2014; Kadko et al., 2019; Moore & Smith, 1986; Nozaki et al., 1976, 1997; J. N. Smith et al., 2003). Asterisks in the legend indicate residence time estimates based on ^{210}Pb .

In the Canada Basin, observed dPb concentrations are slightly elevated (from 3 to 5 pM) in the Atlantic layer (300–800 m; Colombo, Rogalla, et al., 2019). The model captures an increase in dPb concentrations at these depths but underestimates the magnitude by 1–2 pM (Figure 4). This underestimate could be due to stronger adsorptive removal in the model (shorter dPb residence time than in reality), an underestimate of the dPb concentration of the Atlantic Water end-member in the Canada Basin boundary conditions, higher original dPb concentrations in older Atlantic Water, differences in Atlantic Water circulation in the model, or too much mixing in the model. Modeled dPb concentrations at depths below 700 m are low across the domain (0–5 pM), but are higher in the Canada Basin (3–5 pM) than in Baffin Bay (0–3 pM) as a result of the longer dPb residence time in the model in the Canada Basin and the isolation of the deep Baffin Bay in the model (Figure 4).

As noted above, the representation of model concentrations strongly depends on the dPb residence time resulting from the scavenging parameterization (Figure 5). Given the timescale of the model experiments (2002–2021), dPb residence times shorter than 20 years have the most noticeable impact on simulated dPb concentrations, that is, regions shallower than 500–1,000 m and all depths in Baffin Bay. The model captures the anticipated regional variation in dPb residence time: in the upper water column, mean dPb residence time decreases from the Canada Basin to the productive Labrador Sea (Figure 5b). Observed and simulated dPb residence time is shortest in the surface at less than 1 year (Figure 5b; Kadko et al., 2019). At 10–30 m depth, the dPb residence time in the central Arctic Ocean is longer in the model (Figure 5b) than estimated by Kadko et al. (2019). That is not unexpected, as these observational estimates are from summer months when removal is expected to be stronger. Overall, the magnitude of dPb residence time and its change with depth are comparable to observations in a number of ocean basins (Figure 5a). For Baffin Bay, the simulated dPb residence times are short due to high biogenic particle abundances; however, there are no representative observations for this region to constrain the deep water column dPb residence time.

3.2. Sources, Sinks, and Modification of Dissolved Pb in the Canadian Arctic

Dissolved Pb concentrations in the ocean in the Canadian Arctic are controlled by external sources (dissolved and particulate runoff, anthropogenic and natural aerosols delivered directly from the atmosphere and via sea ice, release of sediments in sea ice, and resuspension of sediments), sinks (adsorptive removal), and transport across the model boundaries (western and northern Canada Basin, Hudson Bay, and the Labrador Sea). To gain insight

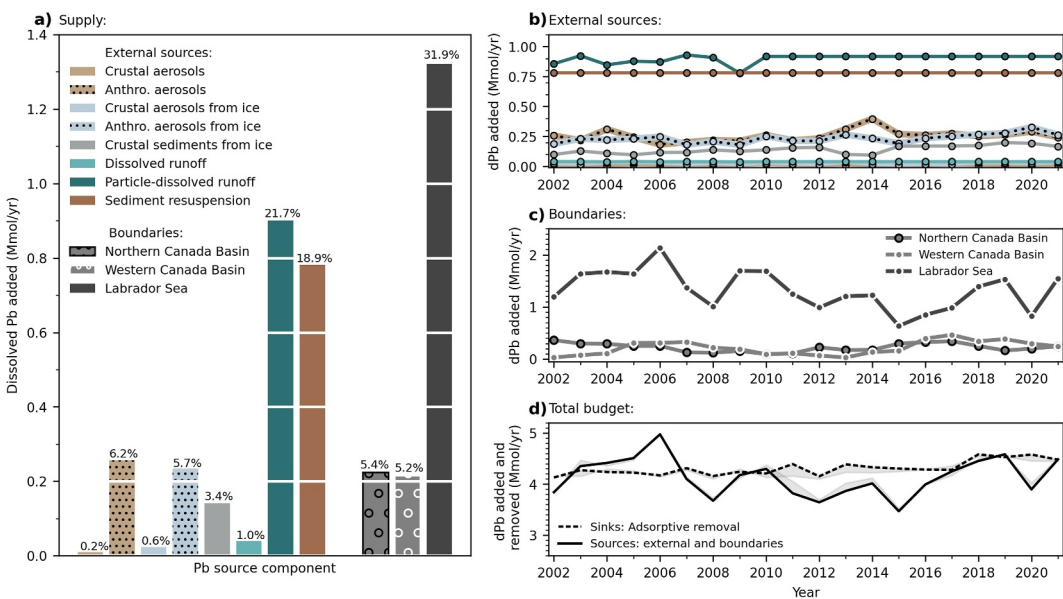


Figure 6. The contributions of the dissolved Pb (dPb) model sources and sinks in the western Arctic Ocean. (a) Annual addition of dPb by source components and net transport across the dPb model domain boundaries (positive values indicate net transport into the domain), averaged from 2002 to 2021. Net transport at the Hudson Bay boundary is too small to appear. The percent labels on top of the bars indicate the proportion that each source contributes to the total dPb addition. Interannual variation of the (b) magnitude of external dPb sources and (c) net transport into the study region. (d) Total magnitude of dPb addition by sources and removal by scavenging within the study domain, with uncertainty from the total budget closure indicated in light gray. Note the different vertical axis scales. We consider the anthropogenic aerosol contributions and at least 50% of dPb transported from the Labrador Sea (Bridgestock et al., 2016) to have a pollution origin, although other external sources such as sediment resuspension and runoff likely have an anthropogenic component as well.

into the relative importance of these processes, we calculate the monthly mean contribution of each component over the reference experiment from 2002 to 2021 (Figure 6), including the net transport of dPb across the model boundaries.

External sources of dPb deliver a total of 2.4 Mmol yr^{-1} or 58% of dPb supplied to the domain (Figures 6a and 6b). Particulate runoff adds 22% of dPb to the ocean surface (varying from 0.8 to 1.0 Mmol yr^{-1}), while dissolved runoff only accounts for 1% of dPb added. The magnitude of dissolved and particulates in runoff varies interannually from 2002 to 2010 and remains constant thereafter, following the model runoff forcing. Sediment resuspension adds 19% of dPb throughout the domain, just above the ocean floor, and there is no source of time variability in the prescription of this process. Anthropogenic aerosols from the atmosphere and sea ice account for 6.2% and 5.7% of dPb addition, respectively, and are more important than the natural fractions (0.2% and 0.6% each). The atmospheric aerosol contributions are maximal in 2004 and 2014, while the sea ice aerosol contributions vary more weakly. Sediments in sea ice contribute 3.4% of dPb to the domain, and its contribution gradually increases over the course of the time series as sea ice melt increases.

The net supply of dPb from the model boundaries to the domain is 1.8 Mmol yr^{-1} and together, the boundaries account for 42% of dPb supply (Figures 6a and 6c). The Labrador Sea is the most important net source of dPb to the domain (1.3 Mmol yr^{-1}), and its supply varies significantly interannually with a maximum of 2.1 Mmol yr^{-1} in 2006 and minimum of 0.6 Mmol yr^{-1} in 2015 (Figure 6c). The western and northern Canada Basin boundaries supply net about 0.2 Mmol yr^{-1} each to the model domain. The Hudson Bay boundary is a small net sink of dPb to the domain ($-0.006 \text{ Mmol yr}^{-1}$); the choice of concentrations at this boundary does not significantly impact the domain as highlighted with a model sensitivity experiment (Figure S4 in Supporting Information S1).

From 2002 to 2021, the modeled annual addition of dPb is mostly less than or equal to the annual modeled removal by scavenging (Figure 6d). As a result, the dPb content within the model domain decreases by 10% over the full time series. The change in dPb content in the model domain is approximately equal to the sum of sources and sinks in the dPb budget. The deviation from complete closure of the budget is shown with light gray shading

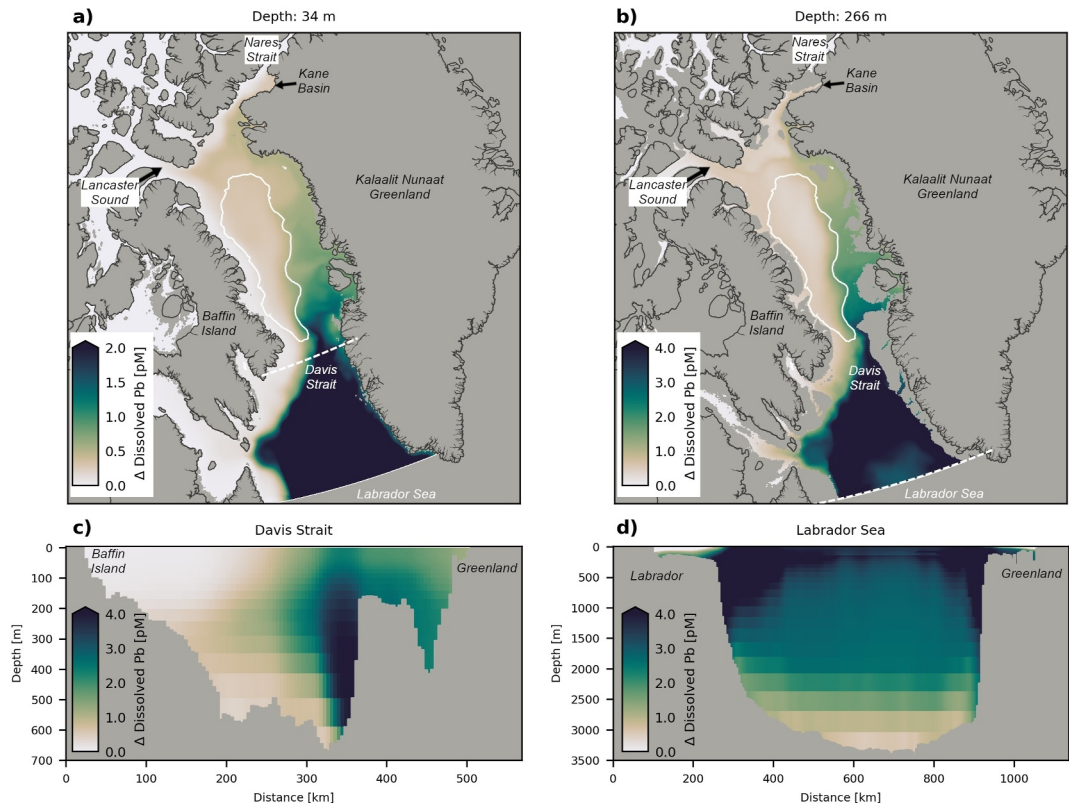


Figure 7. Climatology of the difference in dissolved Pb (ΔdPb) between the “Labrador Atlantic” experiment and the reference experiment at (a) 34 m and (b) 266 m depth (the maximum is 5 pM). The solid white line delineates the 1,000 m isobath. The dashed white lines indicate the locations of cross-sections of (c) Davis Strait and (d) the Labrador Sea. Note the different color bar scale in panel (a) and vertical scales in panel (c) and (d).

in Figure 6d and is likely because the calculation is based on monthly averaged output and does not impact the key findings; the deviation is not due to the seasonality as the model explicitly includes processes driving seasonal dPb cycling. Adsorptive removal varies in a narrow range from 4.1 to 4.6 Mmol yr^{-1} over the time series, while dPb supply ranges from 3.4 to 4.9 Mmol yr^{-1} . The interannual variability of dPb supply in the model primarily depends on the inflow at the Labrador Sea boundary.

3.3. Dissolved Pb as a Tracer of Atlantic Influence in Baffin Bay

Dissolved Pb (dPb) concentrations in Baffin Bay trace the influence of Atlantic Water (Colombo, Rogalla, et al., 2019). We performed a sensitivity experiment of the Labrador Sea boundary condition, called “Labrador Atlantic” (Table 2), to trace Atlantic Water influence (and its associated heat) in Baffin Bay with the dPb model. In this experiment, the dPb concentration of the Atlantic Water end-member (Figures 2a and 2b), which consists primarily of Irminger Water and also Labrador Sea Water, is increased from 30 to 35 pM at the Labrador Sea boundary (altered boundary condition shown in Figure 7d). For the following results, “ Δ dissolved Pb (ΔdPb)” refers to the difference between the dPb concentrations in the Labrador Atlantic and reference experiments (maximum of 5 pM), and is calculated based on a climatology of the time series.

In the Labrador Atlantic experiment, ΔdPb traces well-known pathways of Atlantic influence in Baffin Bay (Figure 7). The cyclonic WGC carries Atlantic Water ($\Delta dPb = 4\text{--}5$ pM) from the Labrador Sea boundary toward Baffin Bay along the Greenland shelf. A large portion of water carried by the WGC recirculates within the Labrador Sea basin and does not cross Davis Strait, as highlighted by the higher ΔdPb concentrations in the Labrador Sea (4–5 pM) than Baffin Bay (0–2 pM). The WGC transports Atlantic-derived Pb to northern Baffin Bay and into Nares Strait north to Kane Basin at all depths ($\Delta dPb = 0.2\text{--}0.8$ pM). Atlantic-derived dPb also highlights the recirculation of water from Baffin Bay along the northern and central part of Lancaster Sound

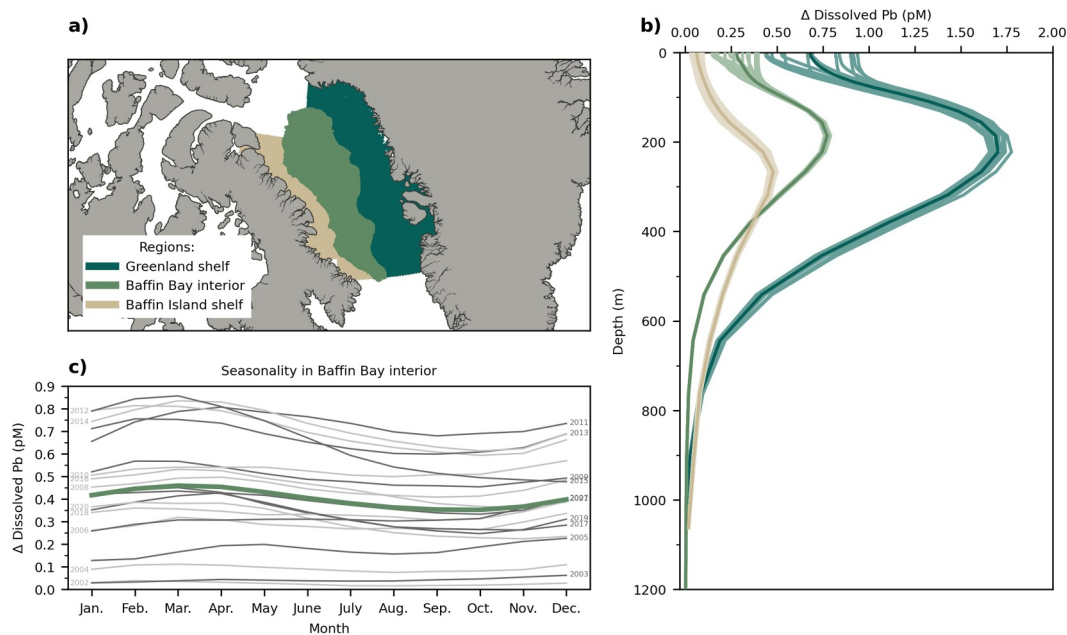


Figure 8. (a) Baffin Bay regions split into the Baffin Bay interior (separated from the continental shelves by the 1,000 m isobath), the Greenland shelf, and the Baffin Island shelf. The northern Baffin Bay shelf is excluded as it is a more complex transition environment. (b) Mean profiles (dark lines) of the difference in dissolved Pb (ΔdPb) in the “Labrador Atlantic” experiment relative to the reference experiment, calculated from climatology over the regions defined in panel (a). Monthly profiles are included in lighter colors and highlight seasonal variability, visible primarily in the upper 100 m. The Baffin Bay interior profile extends to 2,500 m depth with weak Atlantic influence. (c) Seasonal variability in depth-weighted mean ΔdPb for the upper 110 m in the Baffin Bay interior. The thick line reflects the climatology, while the thin lines indicate individual years (light gray are odd years labeled on the left and dark gray are even years labeled on the right), highlighting how dPb propagates throughout the region.

($\Delta dPb = 0.1\text{--}0.4$ pM; Figure 7). In the upper water column, Arctic outflow dilutes the ΔdPb signal on the southern side of Lancaster Sound and along the western side of Nares Strait (Figure 7a). On the Baffin Island shelf, Arctic outflow merges with the WGC and forms the southward flowing Baffin Island Current with weak Atlantic influence ($\Delta dPb = 0\text{--}0.2$ pM compared to $0.4\text{--}0.6$ pM in the WGC in northern Baffin Bay). In Davis Strait, low ΔdPb Arctic outflow dominates the upper 200 m of the western half of the strait, while the northward flowing WGC carries Atlantic influence in the eastern half, with the highest Atlantic-derived dPb content (ΔdPb up to 4 pM) at 150–700 m depth (Figure 7c).

The Labrador Atlantic experiment also shows that the Baffin Bay interior is relatively isolated from Atlantic influence, in particular below 700 m (Figure 8b). The Davis Strait sill is about 640 m deep (670 m in the model) and limits the northward flow of water from the Labrador Sea (Tang et al., 2004). In the Baffin Bay interior, ΔdPb values are nearly zero below the sill depth. Above 100 m depth (Figure 8b), Atlantic influence is strongest on the Greenland shelf ($\Delta dPb = 0.5$ pM), followed by the interior of Baffin Bay ($\Delta dPb = 0.3$ pM), while the influence is much weaker on the Baffin Island shelf ($\Delta dPb = 0.1$ pM). Atlantic influence peaks at a depth of 220 m on the Greenland shelf, 190 m in the Baffin Bay interior, and at 270 m on the Baffin Island shelf (Figure 8b). Atlantic influence on the Baffin Island shelf is weaker than in the other regions, with a maximum ΔdPb of 0.5 pM, and extends deeper in the water column. The Atlantic influence in the upper water column in the Baffin Bay interior varies interannually and has a weak seasonal cycle with a minimum in August and maximum in March (Figure 8c).

The Labrador Atlantic experiment highlights a stronger inflow of Atlantic-derived dPb across Davis Strait each year in the early winter (October–January), and this inflow transports Atlantic Water up the Disko and Uummannaq coastal Greenland troughs (Figure 9; Figures S10 and S11 in Supporting Information S1). The increased inflow of Atlantic Water spans the full water column with strongest dPb concentration increases at the surface and following topography, and is accompanied by stronger northward velocities (Figures 9g and 9h). The timing of this stronger Atlantic Water inflow is consistent with observed increases in Davis Strait (Curry et al., 2014). The

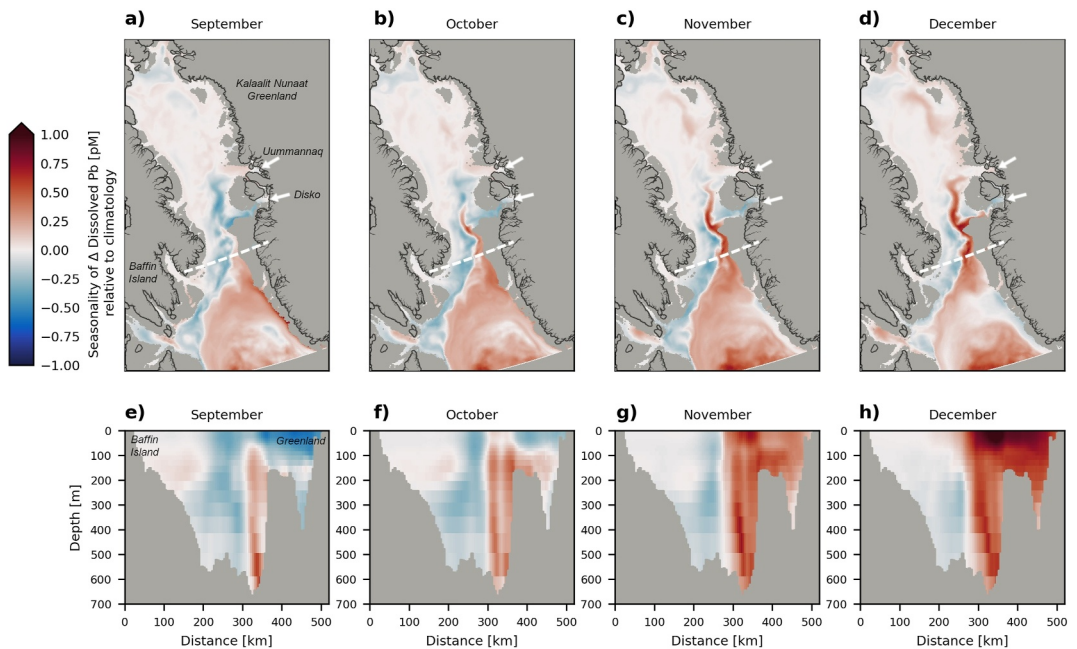


Figure 9. Seasonal variations in inflow of Atlantic-derived dissolved Pb (dPb) to Baffin Bay, highlighted with “ ΔdPb ,” the difference between the Labrador Atlantic and reference experiments (maximum of 5 pM). Panels (a–d) show the monthly difference of ΔdPb at 266 m (the depth of maximum Atlantic influence) from the climatology in Figure 7b. Similarly, panels (e–h) show the monthly difference from the cross-sections in Figure 7c. In panels (a–d), the dashed white line indicates the location of the Davis Strait cross-section (e–h) and the white arrows indicate the heads of the Uummannaq and Disko troughs on the Greenland shelf.

increase in ΔdPb concentrations closely follows the Greenland shelf edge (Figure S10 in Supporting Information S1), and its arrival in Baffin Bay coincides with the seasonal increase in Atlantic influence in the Baffin Bay interior (Figure 8c).

4. Discussion

Over the past decade, observational campaigns have greatly improved our understanding of Pb distributions in the Arctic Ocean (Charette et al., 2020; Colombo, Rogalla, et al., 2019; De Vera, Chandan, Pinedo-González, et al., 2021; Kadko et al., 2019; Vieira et al., 2019). Building on this work, we developed an ocean model of dissolved Pb (dPb) in the Canada Basin, CAA, and Baffin Bay. This dPb model is evaluated with summertime observations, but includes the full seasonal cycle as scavenging varies based on changes to particle abundances and sources such as sea ice melt and boundary transport change in magnitude seasonally. In the following subsections, we use our dPb simulations to discuss the drivers of dPb concentrations in this region in the context of observational studies, identify the importance of advected water masses (and their model representations) for dPb concentrations, and discuss Atlantic Water pathways traced by dPb concentrations.

4.1. Dissolved Pb Cycling in the Canadian Arctic and the Remaining Influence of Anthropogenic Pollution

The dPb model presented here highlights the importance of both natural and anthropogenic sources of dPb, including sources such as particulate matter in runoff, sediment resuspension, and anthropogenic aerosols (Figure 6). In the following, we discuss the importance of these sources as indicated by the dPb model in the context of observational studies.

Sediment resuspension supplied 19% of all dPb added to the Canadian Arctic Ocean in the reference experiment, forming an average contribution of $0.50 \text{ nmol m}^{-2} \text{ day}^{-1}$ (Figure 6). Recent studies in the Arctic Ocean and the North Atlantic have suggested a benthic source of Pb, particularly in shelf regions with strong currents and mixing (De Vera, Chandan, Pinedo-González, et al., 2021; Noble et al., 2015; Rusiecka et al., 2018; Vieira et al., 2019). The exact processes that control benthic dPb release are still under investigation, but sediment resuspension,

release of pore waters, and reductive dissolution from diffusing Mn oxides have been suggested (Noble et al., 2015; Rusiecka et al., 2018; Vieira et al., 2019). However, previous studies have also indicated greater near-bottom removal of dPb due to the increased abundance of particulates near the ocean floor in shelf regions (M. Chen et al., 2012; Lepore et al., 2009; Spencer et al., 1981). Within the CAA, observed dPb profiles did not show a near-bottom increase in dPb concentrations, as were observed for other trace elements such as Fe and Mn, and conditions were not observed to be strongly reducing (Colombo et al., 2020; Colombo, Rogalla, et al., 2019; Rogalla et al., 2022). However, observed dPb concentrations also do not decrease near the seafloor as might be expected in a case without a sedimentary source and with scavenging removal (nonreversible exchange). In the dPb model, concentrations in the lower water column in the CAA are underestimated without sediment resuspension. So, it appears that a net sedimentary source of dPb to the lower water column is required to account for the observed dPb profiles in the CAA. As suggested by De Vera, Chandan, Pinedo-González, et al. (2021), resuspension of sediments enriched in Pb by historical pollution could increase the contribution of this component to the dPb budget in the future.

Particulate matter in runoff has recently been suggested as an important source of dPb to the ocean, accounting for up to 30%–40% of the natural Pb budget globally (M. Chen, Carrasco, et al., 2023). Similarly, Schlosser and Garbe-Schönberg (2019) suggest based on observations that particles and glacial flour can act as a “shuttle” of Pb to the ocean with subsequent release to the dissolved form. In the model, particulate matter in runoff contributes 22% of the dPb supplied to the domain (Figure 6a) and is necessary to represent mixed layer dPb concentrations in regions influenced by glacial runoff, that is, in northern Lancaster Sound, along the Baffin Island coast, and on the west Greenland shelf (Figures 3a and 3d; Rogalla et al., 2023). This estimate of the contribution of particulate runoff to the Arctic is comparable to M. Chen, Carrasco, et al. (2023). In contrast to the particulate fraction, the dissolved Pb fraction in runoff represents only 1% of the model budget. This finding is consistent with studies that suggest that the particulate fraction in runoff can be two orders of magnitude larger than the dissolved fraction (M. Chen, Carrasco, et al., 2023, and references therein). The cycling of Pb along the land-to-sea pathway is complex, and not enough is known to quantify exactly how much dPb adsorbs to particle surfaces and what fraction is removed from suspension at the freshwater/sea interface versus how much dPb is released to the dissolved form in the ocean (Elbaz-Poulichet et al., 1984; Krause et al., 2023; Rusiecka et al., 2018; Schlosser & Garbe-Schönberg, 2019).

It is well established that the Arctic receives Pb from long-range transport of aerosols, especially during the winter Arctic Haze period (De Vera, Chandan, Landing, et al., 2021; Gong & Barrie, 2005; Sharma et al., 2019). In this dPb model, natural and anthropogenic aerosols together contribute 13% of the dPb supplied to the domain via dry and wet atmospheric deposition and flux from sea ice. The average model atmospheric and ice dPb aerosol fluxes are both $0.17 \text{ nmol m}^{-2} \text{ day}^{-1}$, which combine to a total flux of $0.34 \text{ nmol m}^{-2} \text{ day}^{-1}$. Bulk atmospheric deposition fluxes of Pb in the Arctic Ocean and subpolar North Atlantic from observations range from 0.08 to $12 \text{ nmol m}^{-2} \text{ day}^{-1}$, with a commonly assumed rate of approximately $1 \text{ nmol m}^{-2} \text{ day}^{-1}$ (Kadko et al., 2016, 2019; Marsay et al., 2018; Shelley et al., 2017). Thus, the model atmospheric dPb flux is on the lower end of the observed range. Marsay et al. (2018) and De Vera, Chandan, Landing, et al. (2021) attribute most of the Pb in aerosols in the Arctic to anthropogenic sources and found enrichment factors of 10 or greater, comparable to the ratio of anthropogenic to natural aerosols in the dPb model (Figure 6a). Observations of Pb in Greenland snow also show that anthropogenic particles from Europe, North America, and Asia greatly exceed the natural dust fraction (Bory et al., 2014; Lee et al., 2023). Modeled anthropogenic aerosol dPb contributions (derived from black carbon) do not decrease from 2002 to 2021 (Figure 6b). The relative stability of this dPb pollution is consistent with the results of De Vera, Chandan, Landing, et al. (2021), who found that compared to the rapid decline observed in the 1980s and 1990s, the atmospheric pollution of Pb was relatively unchanged since the 2000s.

The fraction of natural versus anthropogenic dPb in Arctic seawater is still under discussion, but isotope ratios in the Canada Basin suggest that anywhere from 25% to 85% of Pb in the water column is of anthropogenic origin (Bridgestock et al., 2016; De Vera, Chandan, Pinedo-González, et al., 2021). The dPb model presented here can give a lower bound estimate of the impact of dPb pollution in the Canadian Arctic Ocean. Anthropogenic aerosols contribute 12% to the dPb budget, and if we assume that 50% of dPb in the North Atlantic is from anthropogenic origin (Bridgestock et al., 2016), the Labrador Sea boundary contributes another 16% anthropogenic dPb to the budget. This gives a lower bound estimate of 28% of dPb in the western Arctic Ocean from pollution. The actual

proportion is likely higher since sediment resuspension and boundary transport from the Pacific are potential secondary sources of dPb pollution (Rudnicka-Kepa & Zaborska, 2021). While runoff may also be impacted by pollution, Pb isotope ratios in CAA rivers are heterogeneous suggesting that external anthropogenic sources do not dominate the Pb composition of runoff (Colombo, Brown, et al., 2019). Similarly, while Pb isotope ratios in ice cores from the Greenland ice sheet identify signatures of anthropogenic Pb pollution (Wensman et al., 2022), observed dPb fluxes in meltwater are primarily associated with dissolution of bedrock and sediments (Krisch et al., 2022). As the net flux of dPb into the study region is greater than the flux out (Figure 6d), the Canadian sector of the Arctic Ocean appears to be a net sink of dPb from pollution supplied directly to the Arctic and indirectly by boundary transport.

4.2. Advection of Dissolved Pb From the Atlantic and Pacific Oceans

dPb concentrations in the Arctic Ocean are much lower (0–6 pM) than the neighboring North Atlantic and North Pacific Oceans, which have received and continued to receive more direct inputs from pollution (Boyle et al., 2014; Kelly et al., 2009; Zurbrick et al., 2017). Strong advective signatures of water from the North Atlantic and Pacific Oceans are observed for dPb within the ocean of the Canadian Arctic (Colombo, Rogalla, et al., 2019). These signatures occur in the dPb model, albeit modified, as discussed below.

Observed dPb concentrations in the North Atlantic Ocean range from 15 to 20 pM in the surface up to 30 pM at intermediate depths (GEOTRACES Intermediate Data Product Group, 2021; Noble et al., 2015; Zurbrick et al., 2018) and enter Baffin Bay through Davis Strait. Atlantic Water transport along the west coast of Greenland displays significant interannual variability (Myers et al., 2007). Advection of high dPb water from the North Atlantic Ocean is the largest contributor of dPb (32%) to the model domain and dominates interannual variability in dPb supply (Figures 6a and 6d). The large net supply of dPb to Baffin Bay from the Labrador Sea boundary in the model also implies that southward transport from Baffin Bay dilutes dPb concentrations in the North Atlantic Ocean. Northward transport from the Labrador Sea boundary by the WGC increases simulated dPb concentrations in the Labrador Sea, Baffin Bay, Nares Strait, and Lancaster Sound (Figures 3 and 7). This finding is unsurprising; Colombo, Rogalla, et al. (2019) observed a peak in dPb concentrations (14–27 pM) in Baffin Bay along a narrow isopycnal surface associated with North Atlantic Water and identified impacts of Atlantic Water in Lancaster Sound.

The relative net contribution of boundary transport to the Canada Basin and CAA is significant but weaker than to the Labrador Sea (5.4% and 5.2% from the western and northern Canada Basin boundaries, respectively). This difference suggests that local dPb supply by external sources such as runoff, resuspension, and aerosols could play a bigger role in dPb cycling in the western Arctic Ocean including the Canada Basin and the CAA. However, the dPb model may also underestimate the role of the Canada Basin boundaries on dPb supply to the model domain as discussed below.

dPb concentrations in the sub-Arctic Pacific Ocean are high (40–50 pM), mainly due to Asian industrial emissions, and enter the Arctic Ocean through Bering Strait (GEOTRACES Intermediate Data Product Group, 2021; Zurbrick et al., 2017). From Bering Strait, Pacific Water flows eastward along the continental shelf in the ACC or across the Chukchi shelf, along the Siberian shelf and into the Transpolar Drift (Aksenov et al., 2016; Spall et al., 2018). Observed dPb concentrations on the highly productive Chukchi shelf are reduced (3–16 pM) relative to the sub-Arctic Pacific, likely due to scavenging (Colombo, Rogalla, et al., 2019; GEOTRACES Intermediate Data Product Group, 2021; Hill et al., 2013). Elevated dPb concentrations (9–16 pM) are observed at 50–100 m depth in the Canada Basin and western CAA, associated with Pacific-derived ACW from the ACC (Colombo, Rogalla, et al., 2019). The dPb model simulates elevated concentrations in the subsurface (Pacific) layer in the Canada Basin, but at 5–7 pM, it underestimates the magnitude of the increase (Figures 3b, 3e, and 4). This discrepancy between observed and simulated dPb concentrations has several possible explanations: the dPb model boundary conditions do not capture ACW appropriately, the dPb concentrations in the ACC are highly variable and can be greater than those observed in the Chukchi shelf region during GEOTRACES GN01, and/or the physical model underestimates Pacific Water transport by the ACC in the years prior to the observations. In the following, we discuss these scenarios.

The underestimation of the subsurface (Pacific) layer peak in simulated dPb is unlikely to be due to the dPb model treatment of the Pacific-derived ACW. ACW enters the dPb model domain via the western Canada Basin boundary (Figure 1) and is identified in the boundary conditions based on its temperature and salinity signature

(details in Section 2.1, Text S1 in Supporting Information S1). We assigned a concentration of 14 pM to the ACW dPb end-member, within the range of 3–16 pM observed in the Bering Strait (GEOTRACES Intermediate Data Product Group, 2021), and thereby set the maximum Pacific Water end-member concentration at the boundary. With our boundary condition metric, ACW is recognized at the Canada Basin boundary from June to October up to 500 km off the Beaufort coast and down to 75 m depth (Figure 2f), and on the Chukchi shelf. Interannual variation in the extent of the ACW does not correlate with changes in the subsurface (Pacific) layer dPb concentrations in subsequent years (transit time is estimated at 2–5 years in X. Hu and Myers (2013)). During tuning, we tested a 4-pM increase in the ACW dPb end-member; however, the simulated concentrations in the subsurface layer in the model domain only increased by a small fraction (approximately 1 pM). Excess adsorptive removal of dPb in the model is unlikely as the mean simulated dPb residence time in the western Arctic Ocean is several years at these depths, potentially longer than observed (Figure 5).

The underestimation of the simulated ACW dPb end-member may suggest that the ACC may not have been fully captured by the GEOTRACES GN01 observations over the Chukchi shelf, or that there could be significant variability in dPb concentrations within the ACC. As water transits from the Chukchi shelf to the interior of the Canada Basin, we would expect a gradual decrease in dPb concentrations due to scavenging removal, yet peak values observed in the subsurface (Pacific) layer in the Canada Basin are as high as, or higher than, those observed on the Chukchi shelf. Observations of particulate Mn and V were unusually elevated in the Pacific layer, potentially influenced by bacteria from the Chukchi shelf, suggesting high abundance of particle surfaces that dPb can adsorb to (Colombo et al., 2022). Typical observed dPb concentrations in the Pacific layer over the Chukchi shelf are between 3 and 6 pM, with two stations nearer the Alaskan coast measuring up to 14 and 16 pM (GEOTRACES Intermediate Data Product Group, 2021). It is possible that GEOTRACES GN01 observations may not have captured the upper maximum dPb concentrations in Pacific Water supplied by the ACC to the Canada Basin and the western CAA. However, observed dPb concentrations in ACW in Bering Strait were not significantly higher (up to 13–16 pM). So, another possibility is that there is strong variation in Bering Strait dPb concentrations, depending on the originating pathways within the Pacific Ocean. The dPb model can not definitively say the observations are missing the maximum dPb concentrations in the ACC; however, it does raise questions about the variability of dPb concentrations flowing in to the Arctic Ocean via Bering Strait.

The underestimation of the simulated subsurface (Pacific) layer dPb concentration can also be used to assess the representation of the transport of ACW in the physical ocean model. The proportion of Pacific Water that follows the Transpolar Drift versus the ACC in the Arctic Ocean varies between ocean models (Aksenov et al., 2016). The most realistic proportion for each of these routes is not well established and is likely to vary considerably interannually. With the same 1/12° configuration, X. Hu et al. (2019) identified that Pacific Water mainly follows the Transpolar Drift from 2002 to 2016, rather than the ACC, suggesting a contributor to the dPb underestimation. The split in supply of ACW between the Transpolar Drift and the ACC can not be the single cause of the dPb underestimation, since the observed 14 pM concentration in the Canada Basin is near the upper maximum observed in Bering Strait and would thus require very direct flow from the boundary. The underestimation of simulated dPb concentrations may also highlight the role of recent observed increases in Bering Strait throughflow (Woodgate, 2018; Woodgate et al., 2012) for the subsurface (Pacific) layer in the Canada Basin.

4.3. Tracing Atlantic Water Pathways in Baffin Bay Using Dissolved Pb

Dissolved Pb (dPb) is a convenient tracer of Atlantic Water due its pollution history; in Baffin Bay, dPb traces well-known pathways of Atlantic influence ([Figure 7; Colombo, Rogalla, et al., 2019; Gobeil et al., 2001]). The Labrador Sea boundary condition in the dPb model identifies the Atlantic Water end-member as mainly Irminger Water within the West Greenland Current (WGC; Pacini et al., 2020). Irminger Water is an important source of heat in Baffin Bay and can drive melt of marine-terminating glaciers, which in turn can shallow and warm the Irminger Water layer in Baffin Bay (Castro de la Guardia et al., 2015; Curry et al., 2014). In the following discussion, we highlight pathways of Atlantic Water within Baffin Bay using “ Δ dissolved Pb (Δ dPb)” as a tracer of the extent and magnitude of influence of Atlantic Water. “ Δ dPb” is defined as the difference between the Labrador Atlantic experiment, with an increased concentration of 5 pM in the Labrador Sea Atlantic Water end-member, and the reference experiment.

In both the model and observations, the cyclonic WGC carries Atlantic Water with anthropogenically elevated dPb concentrations northward along the Greenland coast and combines with outflow from Nares Strait and

Lancaster Sound to flow southward with the Baffin Island Current (Figure 7; Colombo, Rogalla, et al., 2019; Tang et al., 2004). In the model experiments, ΔdPb concentrations gradually decrease and deepen during transit along this pathway as they are diluted by Arctic outflow, mix, and are removed by adsorption (Figure 7). Atlantic influence in Baffin Bay is strongest in the subsurface as identified by peak simulated and observed dPb concentrations and highest simulated values of ΔdPb , and is weak below that due to constraints by the topography (Figures 4 and 8b; Colombo, Rogalla, et al., 2019).

In Nares Strait, ΔdPb indicates consistent spreading of Atlantic influence from the WGC north to Kane Basin (Figures 7a and 7b). On the western side of Nares Strait, a plume of low ΔdPb is visible where Arctic outflow is prevalent. This across-channel difference in ΔdPb concentrations and associated water masses is also apparent in observations with warm salty water on the eastern side of Nares Strait and colder fresher water on the western side (Münchow et al., 2007; Rabe et al., 2010). Periodic flow reversal events could enhance the northward spread of Atlantic Waters in Nares Strait (Myers et al., 2021). In the model, the Atlantic dPb influence within Nares Strait increases below 100 m (ΔdPb up to 1 pM). Observational studies identify mainly Atlantic Water below 100 m at Kennedy Channel north of Kane Basin (Jones & Eert, 2006; Münchow et al., 2007; Rabe et al., 2010), attributed to the Arctic Ocean Atlantic layer. The dPb experiments suggest that in the model, Atlantic Waters in Kane Basin receive contributions from the WGC in addition to the Arctic Ocean Atlantic layer.

The shallow sills in Nares Strait (220 m depth), the CAA (120 m depth), and Davis Strait (640 m depth) isolate the intermediate and deep waters of Baffin Bay from direct connection with the Arctic Ocean and Atlantic Ocean (Tang et al., 2004). Several formation mechanisms have been suggested for deep water in Baffin Bay (summarized by Tang et al. (2004)). In our model, the deep water of Baffin Bay is more or less isolated below the Davis Strait sill (around 670 m in the model), and ΔdPb is very small (Figure 8b). However, ΔdPb is nonzero down to 1,750 m depth, suggesting some weak Atlantic influence. Marson et al. (2017) identify cascading of dense water from Davis Strait, primarily from 2003 to 2006, into Baffin Bay in a $1/4^\circ$ model configuration similar to our configuration. Around 1,245 m depth, a plume of dPb from Atlantic influence crosses Davis Strait into the Baffin Bay interior starting in June and diminishing by November 2004 but is absent later in the time series (Movie S1). Adsorptive removal and mixing depletes this signature in ΔdPb over the following years. So, cascades of dense water from Davis Strait could possibly supply weak Atlantic-derived dPb in the deep interior basin. After 2014, some Atlantic influence occurs along the Baffin Island slope at 1,245 m depth in winter (Movie S1).

Above the Davis Strait sill, ΔdPb highlights strong flow of Atlantic-derived water into Baffin Bay starting in September and lasting through February, inducing a weak seasonal cycle in the Baffin Bay interior in the model (Figures 8c and 9; Figure S11 in Supporting Information S1). The Atlantic Water inflow follows the Greenland continental slope, extends up to the surface, and is strongly controlled by topography (Figure 9; Figure S10 in Supporting Information S1). The period of increased transport of dPb across Davis Strait is preceded by a seasonal increase in total WGC transport and Irminger Water transport from July to January observed near the western tip of Greenland (Curry et al., 2014; Grist et al., 2014; Pacini et al., 2020). Tang et al. (2004) also show strongest northward mean currents in eastern Davis Strait in the fall at all depths. These lines of evidence suggest that the simulated seasonal inflow of Atlantic-derived water, outlined with dPb , is a realistic feature.

Irminger Water transported across Davis Strait by the WGC can supply heat to the Greenland shelf and up Disko and Uummannaq troughs as identified by several studies (Gillard et al., 2020; Gladish et al., 2015; Hansen et al., 2012; Myers & Ribergaard, 2013). Stronger inflow of Atlantic-derived Pb across Davis Strait appears in the dPb model in the early winter (October–January; Figure 9), closely following the bathymetry. The dPb associated with this Atlantic influence extends into the Disko trough and to a lesser extent up to the Uummannaq trough throughout the winter and spring months (Figure S11 in Supporting Information S1). Gillard et al. (2020) identify onshore heat flux from Irminger Water through the Disko trough with a maximum in September–January using a $1/4^\circ$ resolution version of the model configuration used here, matching the arrival of high dPb Irminger Water in the dPb model. While it takes longer for the band of Atlantic-derived dPb to reach the shelf by the Uummannaq trough than the Disko trough because it is farther along the advection pathway (Figure 9; Grist et al., 2014), the up trough spreading appears to occur in December for both troughs via the southern edge (also seen in heat flux by Gillard et al., 2020). Both Disko and Uummannaq troughs transport heat to the Greenland shelf where it can have serious consequences for the marine-terminating glaciers (Gillard et al., 2020; Holland et al., 2008). These regions are also very important for local community fisheries (Jacobsen, 2017), but the seasonal increase in Atlantic-derived Pb supply is unlikely to impact fisheries.

4.4. Limitations

The simulated dissolved Pb (dPb) concentrations, component contributions, and traced Atlantic Water influence depend on the dPb model parameterizations and boundary conditions, and the physical model's representation of Pacific and Atlantic Water transport in the Canada Basin and Baffin Bay (as discussed in Section 4.2). Below, we identify and explain the impact of these factors on the results presented in this study.

The residence time of dPb in the model is set by the scavenging rate (adsorptive removal) and affects the degree of extension of dPb along circulation pathways and the simulated dPb concentrations. The simulated concentrations are most sensitive to the removal rate in regions that are isolated or that have short residence times such as the surface and Baffin Bay (Figure 5). If the modeled residence time of dPb is shorter than in reality, the amount of dPb in the "Labrador Atlantic" experiment would be underestimated. The dPb residence time estimates in the model are comparable to observations on annual timescales, but there is significant variation in the magnitude of observed residence times, and it is challenging to constrain the seasonal variation of removal and its magnitude in coastal regions as observations are sparse or lacking. Further, studies have suggested reversible exchange of dPb, particularly in deep basins that lack strong advective transport and vertically structured water masses (Boyle et al., 2020; Lanning et al., 2023; Noble et al., 2015; Wu et al., 2010). However, reversible exchange can alter Pb isotope ratios without much change in the dissolved Pb concentrations (M. Chen et al., 2016; M. Chen, Boyle, et al., 2023; Lanning et al., 2023). As a result, it is unlikely that reversible scavenging contributes significantly to dPb concentrations in our study region, which also has strong vertical structure and advective signals in the deep Canada Basin and Baffin Bay. The lack of reversible exchange in the dPb model results in weak vertical coupling of dPb, with strongest impact in the deep Canada Basin and Baffin Bay, as the only way for dPb to travel vertically is through advection and mixing. The scavenging rate constant also does not explicitly vary by the particle type, but the parameter β does add a preference of scavenging based on the particle type.

The fractional solubility of Pb is part of all our model parameterizations (except for dissolved Pb in runoff) and is assumed to be constant. The fractional solubility observed and used in other studies covers a broad range from 1% in Schlosser and Garbe-Schönberg (2019), 8% in Henderson and Maier-Reimer (2002), and to 80% in Fishwick et al. (2018) and Lim et al. (1994). Shelley et al. (2018) estimate a typical fractional solubility from 30% to 80% with values covering the full range from 0% to 100%. The fractional solubility used in this study (80%) is on the higher end of the observed ranges, but because the solubility impacts almost all sources, the percent contributions to the budget would remain mostly unchanged (magnitudes would be affected). A potentially more important limitation is that the fractional solubility is the same for all sources, while for example, the solubility of anthropogenic aerosols maybe higher than natural aerosols (Zurbrick et al., 2018). The estimate of the anthropogenic aerosol contribution in the dPb model also assumes a constant ratio of black carbon to anthropogenic Pb. Black carbon has similar but not identical source pathways as anthropogenic Pb (such as biomass burning), so while the ratio appears to have remained relatively constant over time (Sharma et al., 2019), this approach may not capture changes in source regions if applied on longer timescales.

One of the main challenges in both the sediment resuspension and runoff parameterizations is to estimate the magnitude of the net transfer of Pb from particulates to the dissolved Pb pool in the context of the particle reactivity of Pb. The 1/12° resolution of this model is not able to represent the scale of estuarine or local resuspension dynamics, and these processes are highly spatially and temporally variable. Sediment resuspension is expected to vary seasonally due to changing sea ice cover, wind, and storms, but it is represented as a constant process throughout the year, and thus, the dPb model likely underestimates the variability in this component. For runoff in the dPb model, runoff from marine-terminating glaciers is not distinguished from glacial regions drained by rivers. The dynamics of these runoff pathways differ and could impact dPb concentrations nearby Ellesmere Island and on the Greenland shelf. The model also does not resolve subglacial melt plumes, which could entrain higher dPb concentrations from the subsurface ocean around Greenland and Nares Strait and bring these to the surface (Bhatia et al., 2021).

The largest net supply of dPb in the model (42%) is transported into the domain from the boundaries, so the simulated dPb concentrations are sensitive to the choice of water mass end-member concentrations. For this study, we chose to hold the dPb concentrations of the end-members in the boundary conditions constant over time. However, changing pollution patterns impact water mass characteristic dPb properties, and over longer timescales, these would certainly not remain constant. Observations in the Irminger Sea suggest a decrease in dPb at all depths from 1993 to 2014 (Véron et al., 1999; Zurbrick et al., 2018). If the Atlantic end-member in the

Labrador Sea boundary condition decreased over time, dPb concentrations in the Atlantic layer in Baffin Bay would decrease as indicated by the “Labrador Atlantic” experiment. Simulated dPb concentrations in Baffin Bay in 2015 are lower than observed, so it is possible that the Atlantic Water end-member concentration in the boundary is underestimated as it is based on recent observations. Further, while the dPb boundary conditions vary monthly based on which water masses are present, the water mass end-member concentrations are derived from observations in September–October. This assumption is most likely to impact results near the ocean surface close to the open boundaries, where differing particulate contents are likely to induce a seasonal cycle in dPb concentrations in incoming water masses.

While the estimates of the influence of sediment resuspension, particulate runoff, and boundary transport on dPb in the Western Arctic Ocean and Baffin Bay are coarse, the dPb model presented here provides a platform to ask questions about the drivers of dPb concentrations and their likely variability (and potential for change), and outlines pathways of contribution of Atlantic Water and its historical pollution into Baffin Bay. The analysis focused on general questions instead of interannual variability, since the model can only be evaluated with observations in 2015.

5. Conclusions

In this study, we present a model of dissolved Pb (dPb) in the western Arctic Ocean including the Canada Basin, the Canadian Arctic Archipelago (CAA), and Baffin Bay. This model builds on observations collected by the GEOTRACES program (Anderson, 2020), and to the best of our knowledge, this is the first three-dimensional model of dPb in the ocean that includes impacts of anthropogenic pollution. The model captures key features observed in oceanic dPb distributions (Colombo, Rogalla, et al., 2019), including an increase in concentrations from the Canada Basin toward Baffin Bay through the CAA, and an intermediate depth peak in dPb concentrations in Baffin Bay formed by Atlantic Water from the Labrador Sea. With model experiments from 2002 to 2021, we (a) estimate a dPb budget that shows the diversity of dPb sources and (b) trace the pathways of influence of Atlantic Water in Baffin Bay (summarized in Figure 10).

1. The dPb model reveals a diversity of natural and anthropogenic dPb sources that control dPb distributions within the Canadian Arctic. Net transport from the surrounding oceans accounts for 43% of dPb added to the region annually, highlighting the importance of advected water masses for dPb concentrations in the Canadian Arctic. The dPb model underestimates concentrations in advected Pacific-derived Alaskan Coastal Water in the western Arctic, possibly due to strong variability in dPb concentrations in Bering Strait. Particulate matter in runoff supplies 22% of dPb in this model, and this component is likely to be affected by climate-related changes such as increased runoff (Peterson et al., 2002). Aerosols derived from anthropogenic pollution remain important and contribute 12% to simulated dPb addition. Finally, the dPb model suggests that sediment resuspension is necessary (19%) to reproduce observed near-bottom dPb concentrations on the continental shelves of the CAA. In the model, the Canadian sector of the Arctic Ocean is a net sink of dPb with adsorptive removal exceeding local supply, leading to a 10% decrease in dPb concentrations in the Canadian Arctic from 2002 to 2021.
2. Pb has been recognized as a useful tracer of Atlantic Water due to its historical exposure to pollution (Colombo, Rogalla, et al., 2019; Gobeil et al., 2001). With the dPb model, we identify a seasonal (September through January) increase in Atlantic-derived dPb supply to Baffin Bay by the West Greenland Current, which closely follows the topography. This dPb supply traces Atlantic Irminger Water as it spreads up the Disko and Uummannaq troughs to the Greenland coast where the heat of the Atlantic Water can affect marine-terminating glaciers, as identified by Gillard et al. (2020). On the other hand, the deep Baffin Bay interior appears to be largely isolated from Atlantic Water influence and has low Atlantic-derived dPb concentrations. Nevertheless, in the model, a weak supply of dPb from Atlantic Water enters deep Baffin Bay from Davis Strait in 2004. This event is similar to the dense water cascades seen by Marson et al. (2017) and may suggest an episodic supply pathway of Atlantic Water into deep Baffin Bay.

Our dPb model results clarify the mechanisms governing dPb concentrations in the western Arctic Ocean and demonstrate that despite the Arctic Ocean's relative isolation and despite global reductions in Pb pollution, the dPb budget in the Arctic Ocean continues to be impacted by current and historical anthropogenic Pb pollution.

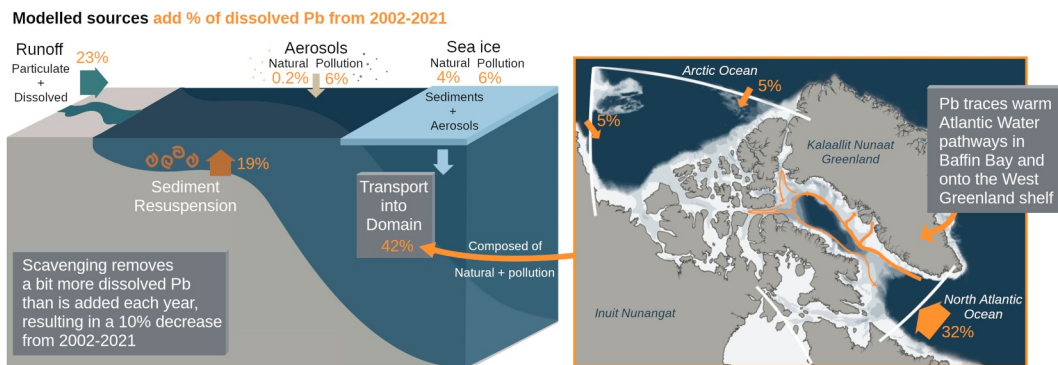


Figure 10. Summary diagram of the key sources of dissolved Pb (dPb) in the western Arctic Ocean with the percent annual addition of dPb averaged over 2002–2021 indicated in orange. The size of the arrows is proportional to the magnitude of contribution from the source.

Data Availability Statement

The dPb model code, configuration, results, and analysis scripts are archived on the Federated Research Data Repository (FRDR) at <https://doi.org/10.20383/103.0965> (Rogalla, 2024). Analysis code is also available on Github at <https://github.com/brogalla/Pb-western-arctic-ocean>. Dissolved Pb observations are available as part of the GEOTRACES Intermediate Data Product Group (2021) via the British Oceanographic Data Centre as follows: <https://www.bodc.ac.uk/geotrades/data/idp2021/>. The numerical ocean model, NEMO, is available at <https://www.nemo-ocean.eu/> (Madec, 2008). For more details on the Arctic and Northern Hemispheric Atlantic 1/12° configuration (ANHA12) of NEMO, visit <https://canadian-nemo-ocean-modelling-forum-community-of-practice.readthedocs.io/en/latest/Institutions/UofA/Configurations/ANHA12/>. All analyses were performed using Python 3 (Van Rossum & Drake, 2009) within Jupyter Notebooks with the NumPy, Pandas, Matplotlib, and cmocean packages (Hunter, 2007; Kluyver et al., 2016; Oliphant, 2006; The Pandas development team, 2020; Thyng et al., 2016). The CESM2 large ensemble data set used for atmosphere, sea ice dust, and black carbon aerosol flux was accessed via the Climate Data Gateway (<https://www.earthsystemgrid.org/dataset/ucar.cgd.cesm2le.output.html>).

Acknowledgments

We would like to acknowledge Stephanie Waterman and Eric Galbraith for their helpful comments on this work. This work was funded by the Natural Sciences and Engineering Council (NSERC) Climate Change and Atmospheric Research Grant: GEOTRACES (RGPC 433848-12), an NSERC Discovery Grant (RGPIN-2016-03865) to SEA, and by the University of British Columbia through a four-year fellowship to BR. Computing resources were provided by the Digital Research Alliance of Canada (RRG 1541 RAC 2021, RRG 1792 RAC 2022, RRG 4603 RAC 2023). We would also like to acknowledge the CESM2 Large Ensemble Community Project, supported by the supercomputing resources provided by the IBS Center for Climate Physics in South Korea.

References

- Aksenov, Y., Karcher, M., Proshutinsky, A., Gerdes, R., De Cuevas, B., Golubeva, E., et al. (2016). Arctic pathways of Pacific Water: Arctic Ocean Model Intercomparison experiments. *Journal of Geophysical Research: Oceans*, 121(1), 27–59. <https://doi.org/10.1002/2015jc011299>
- Anderson, R. F. (2020). GEOTRACES: Accelerating research on the marine biogeochemical cycles of trace elements and their isotopes. *Annual Review of Marine Science*, 12(1), 49–85. <https://doi.org/10.1146/annurev-marine-010318-095123>
- Bacon, M. P., Spencer, D. W., & Brewer, P. G. (1976). ^{210}Pb - ^{226}Ra and ^{210}Po - ^{210}Pb disequilibria in seawater and suspended particulate matter. *Earth and Planetary Science Letters*, 32(2), 277–296. [https://doi.org/10.1016/0012-821x\(76\)90068-6](https://doi.org/10.1016/0012-821x(76)90068-6)
- Bam, W., Maiti, K., Baskaran, M., Krupp, K., Lam, P. J., & Xiang, Y. (2020). Variability in ^{210}Pb and ^{210}Po partition coefficients (Kd) along the US GEOTRACES Arctic transect. *Marine Chemistry*, 219, 103749. <https://doi.org/10.1016/j.marchem.2020.103749>
- Bamber, J., Van Den Broeke, M., Ettema, J., Lenaerts, J., & Rignot, E. (2012). Recent large increases in freshwater fluxes from Greenland into the North Atlantic. *Geophysical Research Letters*, 39(19), L19501. <https://doi.org/10.1029/2012gl052552>
- Bartoňová, L., Raclavská, H., Čech, B., & Kucbel, M. (2019). Behavior of Pb during coal combustion: An overview. *Sustainability*, 11(21), 6061. <https://doi.org/10.3390/su11216061>
- Baskaran, M. (2005). Interaction of sea ice sediments and surface sea water in the Arctic Ocean: Evidence from excess ^{210}Pb . *Geophysical Research Letters*, 32(12), L12601. <https://doi.org/10.1029/2004gl022191>
- Baskaran, M., Krupp, K., Bam, W., & Maiti, K. (2022). Climate change impacts to the Arctic Ocean revealed from high resolution GEOTRACES ^{210}Po - ^{210}Pb - ^{226}Ra disequilibria studies. *Journal of Geophysical Research: Oceans*, 127(5), e2021JC018359. <https://doi.org/10.1029/2021jc018359>
- Bhatia, M. P., Waterman, S., Burgess, D. O., Williams, P. L., Bundy, R. M., Mellett, T., et al. (2021). Glaciers and nutrients in the Canadian Arctic Archipelago marine system. *Global Biogeochemical Cycles*, 35(8), e2021GB006976. <https://doi.org/10.1029/2021gb006976>
- Bolt, C., Aguilar-Islas, A., & Rember, R. (2020). Particulate trace metals in Arctic snow, sea ice, and underlying surface waters during the 2015 US western Arctic GEOTRACES cruise GN01. *ACS Earth and Space Chemistry*, 4(12), 2444–2460. <https://doi.org/10.1021/acsearthspacechem.0c00208>
- Bory, A. J.-M., Abouchami, W., Galer, S. J. G., Svensson, A., Christensen, J. N., & Biscaye, P. E. (2014). A Chinese imprint in insoluble pollutants recently deposited in central Greenland as indicated by lead isotopes. *Environmental Science & Technology*, 48(3), 1451–1457. <https://doi.org/10.1021/es4035655>
- Bouillon, S., Morales Maqueda, M. A., Legat, V., & Fichefet, T. (2009). An elastic-visco-plastic sea ice model formulated on Arakawa B and C grids. *Ocean Modelling*, 27(3–4), 174–184. <https://doi.org/10.1016/j.ocemod.2009.01.004>

- Boutron, C. F., Candelone, J.-P., & Hong, S. (1995). Greenland snow and ice cores: Unique archives of large-scale pollution of the troposphere of the Northern Hemisphere by lead and other heavy metals. *Science of the Total Environment*, 160, 233–241. [https://doi.org/10.1016/0048-9697\(95\)04359-9](https://doi.org/10.1016/0048-9697(95)04359-9)
- Boyle, E. A., Lee, J.-M., Echebeyen, Y., Noble, A., Moos, S., Carrasco, G., et al. (2014). Anthropogenic lead emissions in the ocean: The evolving global experiment. *Oceanography*, 27(1), 69–75. <https://doi.org/10.5670/oceanog.2014.10>
- Boyle, E. A., Zurbrick, C., Lee, J.-M., Till, R., Till, C. P., Zhang, J., & Fleagle, A. R. (2020). Lead and lead isotopes in the US GEOTRACES East Pacific zonal transect (GEOTRACES GP1). *Marine Chemistry*, 227, 103892. <https://doi.org/10.1016/j.marchem.2020.103892>
- Bridgestock, L., Van De Flierdt, T., Rehkämper, M., Paul, M., Middag, R., Milne, A., et al. (2016). Return of naturally sourced Pb to Atlantic surface waters. *Nature Communications*, 7(1), 12921. <https://doi.org/10.1038/ncomms12921>
- Brown, K. A., Williams, W. J., Carmack, E. C., Fiske, G., François, R., McLennan, D., & Peucker-Ehrenbrink, B. (2020). Geochemistry of small Canadian Arctic Rivers with diverse geological and hydrological settings. *Journal of Geophysical Research: Biogeosciences*, 125(1), e2019JG005414. <https://doi.org/10.1029/2019JG005414>
- Cai, M. H., Lin, J., Hong, Q. Q., Wang, Y., & Cai, M. G. (2011). Content and distribution of trace metals in surface sediments from the northern Bering Sea, Chukchi Sea and adjacent Arctic areas. *Marine Pollution Bulletin*, 63(5–12), 523–527. <https://doi.org/10.1016/j.marpolbul.2011.02.007>
- Carrière, L., & Lyard, F. (2003). Modeling the barotropic response of the global ocean to atmospheric wind and pressure forcing—comparisons with observations. *Geophysical Research Letters*, 30(6), 1275. <https://doi.org/10.1029/2002GL016473>
- Castro de la Guardia, L. (2018). *Modelling the response of Arctic and Subarctic marine systems to climate warming* (Doctoral dissertation). University of Alberta. <https://doi.org/10.7939/R31GQ98H>
- Castro de la Guardia, L., Hu, X., & Myers, P. G. (2015). Potential positive feedback between Greenland Ice Sheet melt and Baffin Bay heat content on the west Greenland shelf. *Geophysical Research Letters*, 42(12), 4922–4930. <https://doi.org/10.1002/2015gl064626>
- Charette, M. A., Kipp, L. E., Jensen, L. T., Dabrowski, J. S., Whitmore, L. M., Fitzsimmons, J. N., et al. (2020). The Transpolar Drift as a source of riverine and shelf-derived trace elements to the central Arctic Ocean. *Journal of Geophysical Research: Oceans*, 125(5), e2019JC015920. <https://doi.org/10.1029/2019jc015920>
- Chen, J. H., Wasserburg, G. J., Von Damm, K. L., & Edmond, J. M. (1986). The U-Th-Pb systematics in hot springs on the East Pacific Rise at 21°N and Guaymas Basin. *Geochimica et Cosmochimica Acta*, 50(11), 2467–2479. [https://doi.org/10.1016/0016-7037\(86\)90030-x](https://doi.org/10.1016/0016-7037(86)90030-x)
- Chen, M., Boyle, E. A., Jiang, S., Liu, Q., Zhang, J., Wang, X., & Zhou, K. (2023). Dissolved lead (Pb) concentrations and Pb isotope ratios along the East China Sea and Kuroshio transect—Evidence for isopycnal transport and particle exchange. *Journal of Geophysical Research: Oceans*, 128(2), e2022JC019423. <https://doi.org/10.1029/2022jc019423>
- Chen, M., Boyle, E. A., Lee, J.-M., Nurhati, I., Zurbrick, C., Switzer, A. D., & Carrasco, G. (2016). Lead isotope exchange between dissolved and fluvial particulate matter: A laboratory study from the Johor River estuary. *Philosophical Transactions of the Royal Society A: Mathematical, Physical and Engineering Sciences*, 374(2081), 20160054. <https://doi.org/10.1098/rsta.2016.0054>
- Chen, M., Carrasco, G., Zhao, N., Wang, X., Lee, J. N., Tanzil, J. T., et al. (2023). Boundary exchange completes the marine Pb cycle jigsaw. *Proceedings of the National Academy of Sciences*, 120(6), e2213163120. <https://doi.org/10.1073/pnas.2213163120>
- Chen, M., Ma, Q., Guo, L., Qiu, Y., Li, Y., & Yang, W. (2012). Importance of lateral transport processes to ^{210}Pb budget in the eastern Chukchi Sea during summer 2003. *Deep Sea Research Part II: Topical Studies in Oceanography*, 81, 53–62. <https://doi.org/10.1016/j.dsr.2012.03.011>
- Chuang, C.-Y., Santschi, P. H., Jiang, Y., Ho, Y.-F., Quigg, A., Guo, L., et al. (2014). Important role of biomolecules from diatoms in the scavenging of particle-reactive radionuclides of thorium, protactinium, lead, polonium, and beryllium in the ocean: A case study with Phaeodactylum tricornutum. *Limnology & Oceanography*, 59(4), 1256–1266. <https://doi.org/10.4319/lo.2014.59.4.1256>
- Chung, Y.-J., & Craig, H. (1983). ^{210}Pb in the Pacific: The GEOSECS measurements of particulate and dissolved concentrations. *Earth and Planetary Science Letters*, 65(2), 406–432. [https://doi.org/10.1016/0012-821x\(83\)90179-6](https://doi.org/10.1016/0012-821x(83)90179-6)
- Cochran, J. K., Hirschberg, D. J., Livingston, H. D., Buesseler, K. O., & Key, R. M. (1995). Natural and anthropogenic radionuclide distributions in the Nansen Basin, Arctic Ocean: Scavenging rates and circulation timescales. *Deep Sea Research Part II: Topical Studies in Oceanography*, 42(6), 1495–1517.
- Cochran, J. K., McKibbin-Vaughan, T., Dornblaser, M. M., Hirschberg, D., Livingston, H. D., & Buesseler, K. O. (1990). ^{210}Pb scavenging in the North Atlantic and North Pacific oceans. *Earth and Planetary Science Letters*, 97(3–4), 332–352. [https://doi.org/10.1016/0012-821x\(90\)90050-8](https://doi.org/10.1016/0012-821x(90)90050-8)
- Colombo, M., Brown, K. A., De Vera, J., Bergquist, B. A., & Orians, K. J. (2019). Trace metal geochemistry of remote rivers in the Canadian Arctic Archipelago. *Chemical Geology*, 525, 479–491. <https://doi.org/10.1016/j.chemgeo.2019.08.006>
- Colombo, M., Jackson, S. L., Cullen, J. T., & Orians, K. J. (2020). Dissolved iron and manganese in the Canadian Arctic Ocean: On the biogeochemical processes controlling their distributions. *Geochimica et Cosmochimica Acta*, 277, 150–174. <https://doi.org/10.1016/j.gca.2020.03.012>
- Colombo, M., Li, J., Rogalla, B., Allen, S. E., & Maldonado, M. T. (2022). Particulate trace element distributions along the Canadian Arctic GEOTRACES section: Shelf-water interactions, advective transport and contrasting biological production. *Geochimica et Cosmochimica Acta*, 323, 183–201. <https://doi.org/10.1016/j.gca.2022.02.013>
- Colombo, M., Rogalla, B., Myers, P. G., Allen, S. E., & Orians, K. J. (2019). Tracing dissolved lead sources in the Canadian Arctic: Insights from the Canadian GEOTRACES program. *ACS Earth and Space Chemistry*, 3(7), 1302–1314. <https://doi.org/10.1021/acsearthspacechem.9b00083>
- Courtois, P., Hu, X., Pennelly, C., Spence, P., & Myers, P. G. (2017). Mixed layer depth calculation in deep convection regions in ocean numerical models. *Ocean Modelling*, 120, 60–78. <https://doi.org/10.1016/j.ocemod.2017.10.007>
- Craig, H., Krishnaswami, S., & Somayajulu, B. L. K. (1973). ^{210}Pb - ^{226}Ra : Radioactive disequilibrium in the deep sea. *Earth and Planetary Science Letters*, 17(2), 295–305. [https://doi.org/10.1016/0012-821x\(73\)90194-5](https://doi.org/10.1016/0012-821x(73)90194-5)
- Curry, B., Lee, C. M., Petrie, B., Moritz, R. E., & Kwok, R. (2014). Multiyear volume, liquid freshwater, and sea ice transports through Davis Strait, 2004–10. *Journal of Physical Oceanography*, 44(4), 1244–1266. <https://doi.org/10.1175/jpo-d-13-0177.1>
- Dai, A., Qian, T., Trenberth, K. E., & Milliman, J. D. (2009). Changes in continental freshwater discharge from 1948 to 2004. *Journal of Climate*, 22(10), 2773–2792. <https://doi.org/10.1175/2008jcli2592.1>
- Danabasoglu, G., Deser, C., Rodgers, K., & Timmermann, A. (2022). CESM2 Large Ensemble [Dataset]. NERC EDS British Oceanographic Data Centre NOC. <https://doi.org/10.26024/kgmp-c556>
- De Vera, J., Chandan, P., Landling, W. M., Stupple, G. W., Steffen, A., & Bergquist, B. A. (2021). Amount, sources, and dissolution of aerosol trace elements in the Canadian Arctic. *ACS Earth and Space Chemistry*, 5(10), 2686–2699. <https://doi.org/10.1021/acsearthspacechem.1c00132>
- De Vera, J., Chandan, P., Pinedo-González, P., John, S. G., Jackson, S. L., Cullen, J. T., et al. (2021). Anthropogenic lead pervasive in Canadian Arctic seawater. *Proceedings of the National Academy of Sciences*, 118(24), e2100023118. <https://doi.org/10.1073/pnas.2100023118>

- Duce, R. A., Liss, P. S., Merrill, J. T., Atlas, E. L., Buat-Menard, P., Hicks, B. B., et al. (1991). The atmospheric input of trace species to the world ocean. *Global Biogeochemical Cycles*, 5(3), 193–259. <https://doi.org/10.1029/91gb01778>
- Duinker, J. C. (1983). Effects of particle size and density on the transport of metals to the ocean. In C. S. Wong, E. A. Boyle, K. W. Bruland, J. D. Burton, & E. D. Goldberg (Eds.), *Trace metals in sea water* (Vol. 9, pp. 209–226). Springer.
- Elbaz-Poulichet, F., Holliger, P., Huang, W. W., & Martin, J.-M. (1984). Lead cycling in estuaries, illustrated by the Gironde estuary, France. *Nature*, 308(5958), 409–414. <https://doi.org/10.1038/308409a0>
- Fichefet, T., & Maqueda, M. A. M. (1997). Sensitivity of a global sea ice model to the treatment of ice thermodynamics and dynamics. *Journal of Geophysical Research*, 102(C6), 12609–12646. <https://doi.org/10.1029/97jc00480>
- Fishwick, M. P., Ussher, S. J., Sedwick, P. N., Lohan, M. C., Worsfold, P. J., Buck, K. N., & Church, T. M. (2018). Impact of surface ocean conditions and aerosol provenance on the dissolution of aerosol manganese, cobalt, nickel and lead in seawater. *Marine Chemistry*, 198, 28–43. <https://doi.org/10.1016/j.marchem.2017.11.003>
- Galbraith, E. D., Gnanadesikan, A., Dunne, J. P., & Hiscock, M. R. (2010). Regional impacts of iron-light colimation in a global biogeochemical model. *Biogeochemistry*, 97(3), 1043–1064. <https://doi.org/10.5194/bg-7-1043-2010>
- Gent, P. R., Willebrand, J., McDougall, T. J., & McWilliams, J. C. (1995). Parameterizing eddy-induced tracer transport in ocean circulation models. *Journal of Physical Oceanography*, 25(4), 463–474. [https://doi.org/10.1175/1520-0485\(1995\)025<463:peitt>2.0.co;2](https://doi.org/10.1175/1520-0485(1995)025<463:peitt>2.0.co;2)
- GEOTRACES Intermediate Data Product Group. (2021). The GEOTRACES Intermediate Data Product 2021 (IDP2021) [Dataset]. NERC EDS British Oceanographic Data Centre NOC. <https://doi.org/10.5285/cf2d9ba9-d51d-3b7c-e053-8486abc0f5fd>
- German, C. R., Campbell, A. C., & Edmond, J. M. (1991). Hydrothermal scavenging at the Mid-Atlantic Ridge: Modification of trace element dissolved fluxes. *Earth and Planetary Science Letters*, 107(1), 101–114. [https://doi.org/10.1016/0012-821x\(91\)90047-1](https://doi.org/10.1016/0012-821x(91)90047-1)
- Gillard, L. C., Hu, X., Myers, P. G., Ribergaard, M. H., & Lee, C. M. (2020). Drivers for Atlantic-origin waters abutting Greenland. *The Cryosphere*, 14(8), 2729–2753. <https://doi.org/10.5194/tc-14-2729-2020>
- Gladish, C. V., Holland, D. M., & Lee, C. M. (2015). Oceanic boundary conditions for Jakobshavn Glacier. Part II: Provenance and sources of variability of Disko Bay and Ilulissat ice fjord waters, 1990–2011. *Journal of Physical Oceanography*, 45(1), 33–63. <https://doi.org/10.1175/jpo-d-14-0045.1>
- Gobeil, C., Macdonald, R. W., Smith, J. N., & Beaudin, L. (2001). Atlantic water flow pathways revealed by lead contamination in Arctic basin sediments. *Science*, 293(5533), 1301–1304. <https://doi.org/10.1126/science.1062167>
- Gong, S. L., & Barrie, L. A. (2005). Trends of heavy metal components in the Arctic aerosols and their relationship to the emissions in the Northern Hemisphere. *Science of the Total Environment*, 342(1–3), 175–183. <https://doi.org/10.1016/j.scitotenv.2004.12.031>
- Gong, S. L., Zhao, T. L., Sharma, S., Toom-Sauntry, D., Lavoué, D., Zhang, X. B., et al. (2010). Identification of trends and interannual variability of sulfate and black carbon in the Canadian High Arctic: 1981–2007. *Journal of Geophysical Research*, 115(D7), D07305. <https://doi.org/10.1029/2009jd012943>
- Grist, J. P., Josey, S. A., Boehme, L., Meredith, M. P., Laidre, K. L., Heide-Jørgensen, M. P., et al. (2014). Seasonal variability of the warm Atlantic water layer in the vicinity of the Greenland shelf break. *Geophysical Research Letters*, 41(23), 8530–8537. <https://doi.org/10.1002/2014gl062051>
- Grousset, F. E., Quetel, C. R., Thomas, B., Donard, O. F. X., Lambert, C. E., Guillard, F., & Monaco, A. (1995). Anthropogenic vs. lithogenic origins of trace elements (As, Cd, Pb, Rb, Sb, Sc, Sn, Zn) in water column particles: Northwestern Mediterranean Sea. *Marine Chemistry*, 48(3–4), 291–310. [https://doi.org/10.1016/0304-4203\(94\)00056-j](https://doi.org/10.1016/0304-4203(94)00056-j)
- Hansen, M. O., Nielsen, T. G., Stedmon, C. A., & Munk, P. (2012). Oceanographic regime shift during 1997 in Disko Bay, western Greenland. *Limnology & Oceanography*, 57(2), 634–644. <https://doi.org/10.4319/lo.2012.57.2.0634>
- Hawkins, J. R., Skidmore, M. L., Wadham, J. L., Priscu, J. C., Morton, P. L., Hatton, J. E., et al. (2020). Enhanced trace element mobilization by earth's ice sheets. *Proceedings of the National Academy of Sciences*, 117(50), 31648–31659. <https://doi.org/10.1073/pnas.2014378117>
- Henderson, G. M., & Maier-Reimer, E. (2002). Advection and removal of ^{210}Pb and stable Pb isotopes in the oceans: A general circulation model study. *Geochimica et Cosmochimica Acta*, 66(2), 257–272. [https://doi.org/10.1016/s0016-7037\(01\)00779-7](https://doi.org/10.1016/s0016-7037(01)00779-7)
- Hill, V. J., Matrai, P. A., Olson, E., Suttles, S., Steele, M., Codispoti, L. A., & Zimmerman, R. C. (2013). Synthesis of integrated primary production in the Arctic Ocean: II. In situ and remotely sensed estimates. *Progress in Oceanography*, 110, 107–125. <https://doi.org/10.1016/j.pocean.2012.11.005>
- Holland, D. M., Thomas, R. H., De Young, B., Ribergaard, M. H., & Lyberth, B. (2008). Acceleration of Jakobshavn Isbrae triggered by warm subsurface ocean waters. *Nature Geoscience*, 1(10), 659–664. <https://doi.org/10.1038/ngeo316>
- Hollister, A. P., Kerr, M., Malkki, K., Muhlbach, E., Robert, M., Tilney, C. L., et al. (2020). Regeneration of macronutrients and trace metals during phytoplankton decay: An experimental study. *Limnology & Oceanography*, 65(8), 1936–1960. <https://doi.org/10.1002/lo.11429>
- Hu, W., Chen, M., Yang, W., Zhang, R., Qiu, Y., & Zheng, M. (2014). Low ^{210}Pb in the upper thermocline in the Canadian Basin: Scavenge process over the Chukchi Sea. *Acta Oceanologica Sinica*, 33(6), 28–39. <https://doi.org/10.1007/s13131-014-0486-6>
- Hu, X., & Myers, P. G. (2013). A Lagrangian view of Pacific water inflow pathways in the Arctic Ocean during model spin-up. *Ocean Modelling*, 71, 66–80. <https://doi.org/10.1016/j.ocemod.2013.06.007>
- Hu, X., Myers, P. G., & Lu, Y. (2019). Pacific Water pathway in the Arctic Ocean and Beaufort Gyre in two simulations with different horizontal resolutions. *Journal of Geophysical Research: Oceans*, 124(8), 6414–6432. <https://doi.org/10.1029/2019jc015111>
- Hu, X., Sun, J., Chan, T. O., & Myers, P. G. (2018). Thermodynamic and dynamic ice thickness contributions in the Canadian Arctic Archipelago in NEMO-LIM2 numerical simulations. *The Cryosphere*, 12(4), 1233–1247. <https://doi.org/10.5194/tc-12-1233-2018>
- Hughes, K. G., Klymak, J. M., Hu, X., & Myers, P. G. (2017). Water mass modification and mixing rates in a 1/12 simulation of the Canadian Arctic Archipelago. *Journal of Geophysical Research: Oceans*, 122(2), 803–820. <https://doi.org/10.1002/2016jc012235>
- Hunter, J. D. (2007). Matplotlib: A 2D graphics environment [Software]. *Computer Science and Engineering*, 9(3), 90–95. <https://doi.org/10.1109/mcse.2007.55>
- Jacobsen, R. B. (2017). Befolkningsens holdninger til fiskeriets rolle i det grønlandske samfund: Rapport til grønlandske borgere og interesser i fiskeriet. Retrieved from <https://vbn.aau.dk/en/publications/befolkningsens-holdninger-til-fiskeriets-rolle-i-det-gr%C3%83B8nlandske-s>
- Jiann, K.-T., Wen, L.-S., & Santschi, P. H. (2005). Trace metal (Cd, Cu, Ni and Pb) partitioning, affinities and removal in the Danshuei River estuary, a macro-tidal, temporally anoxic estuary in Taiwan. *Marine Chemistry*, 96(3–4), 293–313. <https://doi.org/10.1016/j.marchem.2005.03.001>
- Jones, E. P., & Eert, A. J. (2006). Waters of Nares Strait in 2001. *Polarforschung*, 74(1–3), 185–189.
- Kadko, D., Aguilera-Islas, A., Bolt, C., Buck, C. S., Fitzsimmons, J. N., Jensen, L. T., et al. (2019). The residence times of trace elements determined in the surface Arctic Ocean during the 2015 US Arctic GEOTRACES expedition. *Marine Chemistry*, 208, 56–69. <https://doi.org/10.1016/j.marchem.2018.10.011>

- Kadko, D., Galfond, B., Landing, W. M., & Shelley, R. U. (2016). Determining the pathways, fate, and flux of atmospherically derived trace elements in the Arctic ocean/ice system. *Marine Chemistry*, 182, 38–50. <https://doi.org/10.1016/j.marchem.2016.04.006>
- Kelly, A. E., Reuer, M. K., Goodkin, N. F., & Boyle, E. A. (2009). Lead concentrations and isotopes in corals and water near Bermuda, 1780–2000. *Earth and Planetary Science Letters*, 283(1–4), 93–100. <https://doi.org/10.1016/j.epsl.2009.03.045>
- Kluyver, T., Ragan-Kelley, B., Pérez, F., Granger, B., Bussonnier, M., Frederic, J., et al. (2016). Jupyter Notebooks – A publishing format for reproducible computational workflows [Software]. *IOS Press*. <https://doi.org/10.3233/978-1-61499-649-1-87>
- Krause, J., Zhu, X., Höfer, J., Achterberg, E. P., Engel, A., Meire, L., et al. (2023). Glacier-derived particles as a regional control on marine dissolved Pb concentrations. *Journal of Geophysical Research: Biogeosciences*, 128(10), e2023JG007514. <https://doi.org/10.1029/2023JG007514>
- Krisch, S., Huhn, O., Al-Hashem, A., Hopwood, M. J., Lodeiro, P., & Achterberg, E. P. (2022). Quantifying ice-sheet derived lead (Pb) fluxes to the ocean; a case study at Nioghalvfjerdssbrae. *Geophysical Research Letters*, 49(21), e2022GL100296. <https://doi.org/10.1029/2022gl100296>
- Kuzyk, Z. Z. A., Gobeil, C., & Macdonald, R. W. (2013). ^{210}Pb and ^{137}Cs in margin sediments of the Arctic Ocean: Controls on boundary scavenging. *Global Biogeochemical Cycles*, 27(2), 422–439. <https://doi.org/10.1002/gbc.20041>
- Lambert, C. E., Veron, A., Buat-Menard, P., Heyraud, M., Groussot, F., & Simpson, W. (1991). The role of large biogenic particles in the transport of atmospheric pollutant Pb down to north-Atlantic sediments. *Oceanologica Acta*, 14(1), 67–76.
- Lanning, N. T., Jiang, S., Amaral, V. J., Mateos, K., Steffen, J. M., Lam, P. J., et al. (2023). Isotopes illustrate vertical transport of anthropogenic Pb by reversible scavenging within Pacific Ocean particle veils. *Proceedings of the National Academy of Sciences*, 120(23), e2219688120. <https://doi.org/10.1073/pnas.2219688120>
- Lee, S., Lee, K., Han, C., Han, Y., Hong, S.-B., Do Hur, S., et al. (2023). Recent decline in atmospheric Pb deposition and isotopic constraints on changes in source contributions in snow from northwestern Greenland. *Chemosphere*, 345, 140441. <https://doi.org/10.1016/j.chemosphere.2023.140441>
- Lepore, K., Moran, S. B., & Smith, J. N. (2009). ^{210}Pb as a tracer of shelf–basin transport and sediment focusing in the Chukchi Sea. *Deep Sea Research Part II: Topical Studies in Oceanography*, 56(17), 1305–1315. <https://doi.org/10.1016/j.dsr2.2008.10.021>
- Lévy, M., Estublier, A., & Madec, G. (2001). Choice of an advection scheme for biogeochemical models. *Geophysical Research Letters*, 28(19), 3725–3728. <https://doi.org/10.1029/2001gl012947>
- Lim, B., Jickells, T. D., Colin, J. L., & Losno, R. (1994). Solubilities of Al, Pb, Cu, and Zn in rain sampled in the marine environment over the North Atlantic Ocean and Mediterranean Sea. *Global Biogeochemical Cycles*, 8(3), 349–362. <https://doi.org/10.1029/94gb01267>
- Luengen, A. C., Raimondi, P. T., & Flagel, A. R. (2007). Contrasting biogeochemistry of six trace metals during the rise and decay of a spring phytoplankton bloom in San Francisco Bay. *Limnology & Oceanography*, 52(3), 1112–1130. <https://doi.org/10.4319/lo.2007.52.3.1112>
- Macdonald, R. W., Barrie, L. A., Bidleman, T. F., Diamond, M. L., Gregor, D. J., Semkin, R. G., et al. (2000). Contaminants in the Canadian Arctic: 5 years of progress in understanding sources, occurrence and pathways. *Science of the Total Environment*, 254(2–3), 93–234. [https://doi.org/10.1016/s0048-9697\(00\)00434-4](https://doi.org/10.1016/s0048-9697(00)00434-4)
- Madec, G. (2008). *NEMO ocean engine, Note du Pôle de modélisation* (Vol. 27). Institut Pierre-Simon Laplace. Retrieved from https://www.nemo-ocean.eu/wp-content/uploads/NEMO_book.pdf
- Marsay, C. M., Aguilar-Islas, A., Fitzsimmons, J. N., Hatta, M., Jensen, L. T., John, S. G., et al. (2018). Dissolved and particulate trace elements in late summer Arctic melt ponds. *Marine Chemistry*, 204, 70–85. <https://doi.org/10.1016/j.marchem.2018.06.002>
- Marson, J. M., Myers, P. G., Hu, X., Petrie, B., Azetsu-Scott, K., & Lee, C. M. (2017). Cascading off the West Greenland Shelf: A numerical perspective. *Journal of Geophysical Research: Oceans*, 122(7), 5316–5328. <https://doi.org/10.1002/2017JC012801>
- Moore, R. M., & Smith, J. N. (1986). Disequilibria between ^{226}Ra , ^{210}Pb and ^{210}Po in the Arctic Ocean and the implications for chemical modification of the Pacific water inflow. *Earth and Planetary Science Letters*, 77(3–4), 285–292. [https://doi.org/10.1016/0012-821x\(86\)90140-8](https://doi.org/10.1016/0012-821x(86)90140-8)
- Münchow, A., Falkner, K. K., & Melling, H. (2007). Spatial continuity of measured seawater and tracer fluxes through Nares Strait, a dynamically wide channel bordering the Canadian Archipelago. *Journal of Marine Research*, 65(6), 759–788. <https://doi.org/10.1357/002224007784219048>
- Myers, P. G., Castro de la Guardia, L., Fu, C., Gillard, L. C., Grivault, N., Hu, X., et al. (2021). Extreme high Greenland Blocking Index leads to the reversal of Davis and Nares Strait net transport toward the Arctic Ocean. *Geophysical Research Letters*, 48(17), e2021GL094178. <https://doi.org/10.1029/2021gl094178>
- Myers, P. G., Kulan, N., & Ribergaard, M. H. (2007). Irminger water variability in the West Greenland Current. *Geophysical Research Letters*, 34(17), L17601. <https://doi.org/10.1029/2007gl030419>
- Myers, P. G., & Ribergaard, M. H. (2013). Warming of the polar water layer in Disko Bay and potential impact on Jakobshavn Isbrae. *Journal of Physical Oceanography*, 43(12), 2629–2640. <https://doi.org/10.1175/jpo-d-12-051.1>
- Nag, R., & Cummins, E. (2022). Human health risk assessment of lead (Pb) through the environmental-food pathway. *Science of the Total Environment*, 810, 151168. <https://doi.org/10.1016/j.scitotenv.2021.151168>
- Noble, A. E., Echegeoyen-Sanz, Y., Boyle, E. A., Ohnemus, D. C., Lam, P. J., Kayser, R., et al. (2015). Dynamic variability of dissolved Pb and Pb isotope composition from the US North Atlantic GEOTRACES transect. *Deep Sea Research Part II: Topical Studies in Oceanography*, 116, 208–225. <https://doi.org/10.1016/j.dsr2.2014.11.011>
- Nozaki, Y., Thomson, J., & Turekian, K. K. (1976). The distribution of ^{210}Pb and ^{210}Po in the surface waters of the Pacific Ocean. *Earth and Planetary Science Letters*, 32(2), 304–312. [https://doi.org/10.1016/0012-821x\(76\)90070-4](https://doi.org/10.1016/0012-821x(76)90070-4)
- Nozaki, Y., Zhang, J., & Takeda, A. (1997). ^{210}Pb and ^{210}Po in the equatorial Pacific and the Bering Sea: The effects of biological productivity and boundary scavenging. *Deep Sea Research Part II: Topical Studies in Oceanography*, 44(9–10), 2203–2220. [https://doi.org/10.1016/s0967-0645\(97\)00024-6](https://doi.org/10.1016/s0967-0645(97)00024-6)
- Oiphant, T. E. (2006). A guide to NumPy [Software]. *Trelgol Publishing USA*, 1. <https://web.mit.edu/dvp/Public/numpybook.pdf>
- Pacini, A., Pickart, R. S., Bahr, F., Torres, D. J., Ramsey, A. L., Holte, J., et al. (2020). Mean conditions and seasonality of the west Greenland boundary current system near Cape Farewell. *Journal of Physical Oceanography*, 50(10), 2849–2871. <https://doi.org/10.1175/jpo-d-20-0086.1>
- Patterson, C. C., & Settle, D. M. (1987a). Magnitude of lead flux to the atmosphere from volcanoes. *Geochimica et Cosmochimica Acta*, 51(3), 675–681. [https://doi.org/10.1016/0016-7037\(87\)90078-0](https://doi.org/10.1016/0016-7037(87)90078-0)
- Patterson, C. C., & Settle, D. M. (1987b). Review of data on eolian fluxes of industrial and natural lead to the lands and seas in remote regions on a global scale. *Marine Chemistry*, 22(2–4), 137–162. [https://doi.org/10.1016/0304-4203\(87\)90005-3](https://doi.org/10.1016/0304-4203(87)90005-3)
- Peterson, B. J., Holmes, R. M., McClelland, J. W., Vörösmarty, C. J., Lammers, R. B., Shiklomanov, A. I., et al. (2002). Increasing river discharge to the Arctic Ocean. *Science*, 298(5601), 2171–2173. <https://doi.org/10.1126/science.1077445>
- Pfirman, S. L., Eicken, H., Bauch, D., & Weeks, W. F. (1995). The potential transport of pollutants by Arctic sea ice. *Science of the Total Environment*, 159(2–3), 129–146. [https://doi.org/10.1016/0048-9697\(95\)04174-y](https://doi.org/10.1016/0048-9697(95)04174-y)

- Pinedo-González, P., West, A. J., Tovar-Sánchez, A., Duarte, C. M., & Sañudo-Wilhelmy, S. A. (2018). Concentration and isotopic composition of dissolved Pb in surface waters of the modern global ocean. *Geochimica et Cosmochimica Acta*, 235, 41–54. <https://doi.org/10.1016/j.gca.2018.05.005>
- Rabe, B., Münchow, A., Johnson, H. L., & Melling, H. (2010). Nares Strait hydrography and salinity field from a 3-year moored array. *Journal of Geophysical Research*, 115(C7), C07010. <https://doi.org/10.1029/2009jc005966>
- Rodgers, K. B., Lee, S.-S., Rosenbloom, N., Timmermann, A., Danabasoglu, G., Deser, C., et al. (2021). Ubiquity of human-induced changes in climate variability. *Earth System Dynamics*, 12(4), 1393–1411. <https://doi.org/10.5194/esd-12-1393-2021>
- Rogalla, B. (2024). Dissolved lead (Pb) in the Western Arctic Ocean and Baffin Bay - Model output and code for Rogalla et al. 2024 [Dataset]. *Federated Research Data Repository*. <https://doi.org/10.20383/103.0965>
- Rogalla, B., Allen, S. E., Colombo, M., Myers, P. G., & Orians, K. J. (2022). Sediments in sea ice drive the Canada Basin surface Mn maximum: Insights from an Arctic Mn ocean model. *Global Biogeochemical Cycles*, 36(8), e2022GB007320. <https://doi.org/10.1002/essoar.10507013.3>
- Rogalla, B., Allen, S. E., Colombo, M., Myers, P. G., & Orians, K. J. (2023). Continental and glacial runoff fingerprints in the Canadian Arctic Archipelago, the Inuit Nunangat Ocean. *Journal of Geophysical Research: Biogeosciences*, 128(5), e2022JG007072. <https://doi.org/10.1029/2022JG007072>
- Rosman, K. J. R., Chisholm, W., Boutron, C. F., Candelone, J. P., & Görlich, U. (1993). Isotopic evidence for the source of lead in Greenland snows since the late 1960s. *Nature*, 362(6418), 333–335. <https://doi.org/10.1038/36233a0>
- Rudnicka-Kepa, P., & Zaborska, A. (2021). Sources, fate and distribution of inorganic contaminants in the Svalbard area, representative of a typical Arctic critical environment—A review. *Environmental Monitoring and Assessment*, 193(11), 724. <https://doi.org/10.1007/s10661-021-09305-6>
- Rusiecka, D., Gledhill, M., Milne, A., Achterberg, E. P., Annett, A. L., Atkinson, S., et al. (2018). Anthropogenic signatures of lead in the Northeast Atlantic. *Geophysical Research Letters*, 45(6), 2734–2743. <https://doi.org/10.1002/2017gl076825>
- Schaule, B. K., & Patterson, C. C. (1981). Lead concentrations in the northeast Pacific: Evidence for global anthropogenic perturbations. *Earth and Planetary Science Letters*, 54(1), 97–116. [https://doi.org/10.1016/0012-821x\(81\)90072-8](https://doi.org/10.1016/0012-821x(81)90072-8)
- Schlosser, C., & Garbe-Schönberg, D. (2019). Mechanisms of Pb supply and removal in two remote (sub-) polar ocean regions. *Marine Pollution Bulletin*, 149, 110659.
- Sharma, S., Barrie, L. A., Magnusson, E., Brattström, G., Leaitch, W. R., Steffen, A., & Landsberger, S. (2019). A factor and trends analysis of multidecadal lower tropospheric observations of Arctic aerosol composition, black carbon, ozone, and mercury at Alert, Canada. *Journal of Geophysical Research: Atmospheres*, 124(24), 14133–14161. <https://doi.org/10.1029/2019jd030844>
- Shelley, R. U., Landing, W. M., Ussher, S. J., Planquette, H., & Sarthou, G. (2018). Regional trends in the fractional solubility of Fe and other metals from North Atlantic aerosols (GEOTRACES cruises GA01 and GA03) following a two-stage leach. *Biogeosciences*, 15(8), 2271–2288. <https://doi.org/10.5194/bg-15-2271-2018>
- Shelley, R. U., Roca-Martí, M., Castrillejo, M., Sanial, V., Masqué, P., Landing, W. M., et al. (2017). Quantification of trace element atmospheric deposition fluxes to the Atlantic Ocean (>40°N; GEOVIDE, GEOTRACES GA01) during spring 2014. *Deep Sea Research Part I: Oceanographic Research Papers*, 119, 34–49.
- Shotyk, W., Zheng, J., Krachler, M., Zdanowicz, C., Koerner, R., & Fisher, D. (2005). Predominance of industrial Pb in recent snow (1994–2004) and ice (1842–1996) from Devon Island, Arctic Canada. *Geophysical Research Letters*, 32(21), L21814. <https://doi.org/10.1029/2005gl023860>
- Sirois, A., & Barrie, L. A. (1999). Arctic lower tropospheric aerosol trends and composition at Alert, Canada: 1980–1995. *Journal of Geophysical Research*, 104(D9), 11599–11618. <https://doi.org/10.1029/1999jd900077>
- Smith, G. C., Roy, F., Mann, P., Dupont, F., Brasnett, B., Lemieux, J.-F., et al. (2014). A new atmospheric dataset for forcing ice-ocean models: Evaluation of reforecasts using the Canadian global deterministic prediction system. *Quarterly Journal of the Royal Meteorological Society*, 140(680), 881–894. <https://doi.org/10.1002/qj.2194>
- Smith, J. N., Moran, S. B., & Macdonald, R. W. (2003). Shelf-basin interactions in the Arctic Ocean based on ^{210}Pb and Ra isotope tracer distributions. *Deep Sea Research Part I: Oceanographic Research Papers*, 50(3), 397–416. [https://doi.org/10.1016/s0967-0637\(02\)00166-8](https://doi.org/10.1016/s0967-0637(02)00166-8)
- Spall, M. A., Pickart, R. S., Li, M., Itoh, M., Lin, P., Kikuchi, T., & Qi, Y. (2018). Transport of Pacific water into the Canada Basin and the formation of the Chukchi slope current. *Journal of Geophysical Research: Oceans*, 123(10), 7453–7471. <https://doi.org/10.1029/2018jc013825>
- Spencer, D. W., Bacon, M. P., & Brewer, P. G. (1981). Models of the distribution of ^{210}Pb in a section across the North Equatorial Atlantic Ocean. *Journal of Marine Research*, 39(1), 119–138.
- Sturges, W. T., & Barrie, L. A. (1989). Stable lead isotope ratios in Arctic aerosols: Evidence for the origin of Arctic air pollution. *Atmospheric Environment*, 23(11), 2513–2519. [https://doi.org/10.1016/0004-6981\(89\)90263-1](https://doi.org/10.1016/0004-6981(89)90263-1)
- Tang, C. C. L., Ross, C. K., Yao, T., Petrie, B., DeTracey, B. M., & Dunlap, E. (2004). The circulation, water masses and sea-ice of Baffin Bay. *Progress in Oceanography*, 63(4), 183–228. <https://doi.org/10.1016/j.pocean.2004.09.005>
- The Pandas development team. (2020). Pandas-dev/pandas: Pandas [Software]. Zenodo, 21, 1–9.
- Thibodeau, B., Migon, C., Dufour, A., Poirier, A., Mari, X., Ghaleb, B., & Legendre, L. (2017). Low sedimentary accumulation of lead caused by weak downward export of organic matter in Hudson Bay, northern Canada. *Biogeochemistry*, 136(3), 279–291. <https://doi.org/10.1007/s10533-017-0395-9>
- Thyng, K. M., Greene, C. A., Hetland, R. D., Zimmerle, H. M., & DiMarco, S. F. (2016). True colors of oceanography: Guidelines for effective and accurate colormap selection [Software]. *Oceanography*, 29(3), 9–13. <https://doi.org/10.5670/oceanog.2016.66>
- Van Rossum, G., & Drake, F. L. (2009). Python 3 Reference Manual [Software]. CreateSpace. Retrieved from <https://dl.acm.org/doi/abs/10.5555/1593487>
- Véron, A. J., Church, T. M., Rivera-Duarte, I., & Flegal, A. R. (1999). Stable lead isotopic ratios trace thermohaline circulation in the subarctic North Atlantic. *Deep Sea Research Part II: Topical Studies in Oceanography*, 46(5), 919–935. [https://doi.org/10.1016/s0967-0645\(99\)00009-0](https://doi.org/10.1016/s0967-0645(99)00009-0)
- Vieira, L. H., Achterberg, E. P., Scholten, J., Beck, A. J., Liebetrau, V., Mills, M. M., & Arrigo, K. R. (2019). Benthic fluxes of trace metals in the Chukchi Sea and their transport into the Arctic Ocean. *Marine Chemistry*, 208, 43–55. <https://doi.org/10.1016/j.marchem.2018.11.001>
- Wedepohl, H. K. (1995). The composition of the continental crust. *Geochimica et Cosmochimica Acta*, 59(7), 1217–1232.
- Wensman, S. M., Shiel, A. E., & McConnell, J. R. (2022). Lead isotopic fingerprinting of 250-years of industrial era pollution in Greenland ice. *Anthropocene*, 38, 100340. <https://doi.org/10.1016/j.ancene.2022.100340>
- Woodgate, R. A. (2018). Increases in the Pacific inflow to the Arctic from 1990 to 2015, and insights into seasonal trends and driving mechanisms from year-round Bering Strait mooring data. *Progress in Oceanography*, 160, 124–154. <https://doi.org/10.1016/j.pocean.2017.12.007>
- Woodgate, R. A., Weingartner, T. J., & Lindsay, R. (2012). Observed increases in Bering Strait oceanic fluxes from the Pacific to the Arctic from 2001 to 2011 and their impacts on the Arctic Ocean water column. *Geophysical Research Letters*, 39(24), L24603. <https://doi.org/10.1029/2012gl054092>

- Wu, J., Rember, R., Jin, M., Boyle, E. A., & Flegal, A. R. (2010). Isotopic evidence for the source of lead in the North Pacific abyssal water. *Geochimica et Cosmochimica Acta*, 74(16), 4629–4638. <https://doi.org/10.1016/j.gca.2010.05.017>
- Xiang, Y., & Lam, P. J. (2020). Size-fractionated compositions of marine suspended particles in the Western Arctic Ocean: Lateral and vertical sources. *Journal of Geophysical Research: Oceans*, 125(8), e2020JC016144. <https://doi.org/10.1029/2020jc016144>
- Zurbrick, C. M., Boyle, E. A., Kayser, R. J., Reuer, M. K., Wu, J., Planquette, H., et al. (2018). Dissolved Pb and Pb isotopes in the North Atlantic from the GEOVIDE transect (GEOTRACES GA-01) and their decadal evolution. *Biogeochemistry*, 135(16), 4995–5014. <https://doi.org/10.5194/bg-15-4995-2018>
- Zurbrick, C. M., Gallon, C., & Flegal, A. R. (2017). Historic and industrial lead within the Northwest Pacific Ocean evidenced by lead isotopes in seawater. *Environmental Science & Technology*, 51(3), 1203–1212. <https://doi.org/10.1021/acs.est.6b04666>